A Review of Gold and Silver Nanoparticle-Based Colorimetric Sensing Assays

Myalowenkosi Sabela, Sébastien Balme, Mikhael Bechelany, Jean-Marc Janot, Krishna Bisetty

A Review of Gold and Silver Nanoparticle-Based Colorimetric Sensing Assays

Myalowenkosi Sabela[a], Sebastien Balme[b*], Mikhael Bechelany[b*], Jean-Marc Janot[b], and Krishna Bisetty[a]

[a] Department of Chemistry, Durban University of Technology, P.O Box 1334, Durban 4000, South Africa

[b] Institut Européen des Membranes, UMR 5635, Université de Montpellier CNRS, ENSCM, Place Eugène Bataillon, F-34095 Montpellier cedex 5, France

[*]Corresponding Author s: sebastien.balme@ umontpellier.fr and mikhael.bechelany@umontpellier.fr

Contents

ABSTRACT

The nanoparticle colorimetric-based methods have been extensively used for rapid detection, however there are few limitations which can be kept under control or avoided by understanding the crucial parameters involved in these reactions. This review addresses the main parameters

that influence colorimetric-based methods and provides a rational classification of the current approaches, by focusing particularly on gold nanoparticles (AuNPs) and silver nanoparticles (AgNPs). The AgNP and AuNP-based colorimetric assays can be very efficient and sensitive especially for biomolecule identification and for metal ion detection in environmental screening. Specifically, this review highlights the detection of metal ions through their coordination with nanoparticle stabilizing ligands. The review also addresses various approaches based on label-free aptasensors to better understand their role as smart colorimetric sensing devices.

1. Introduction

The term *nanoparticle* (NP) defines any small object (from 1 to 100 nm) that behaves as a unit concerning its transport and properties. Indeed, as their properties change in function of their size, particles can be classified based on their diameter. Thus, ultrafine particles (or NPs) are particles with a diameter between 1 and 100 nm, whereas fine particles have a diameter between 100 and 2,500 nm. For tailored applications, NPs can be capped with a variety of different anionic and cationic ligands, from displaceable small molecules to polymer coatings. The choice of capping ligand depends on the NPs used that can range from conductive inks to biomedical tools.

Among the known nanoparticles, gold and silver NPs (AuNPs and AgNPs) have been widely studied because of their unique optical, electrical and photothermal properties. AuNPs and AgNPs show unique optical features in well-dispersed solutions, depending on their level of aggregation which is mostly determined by their specific surface plasmon resonance (SPR) profiles [1],. Metal-noble NPs are small enough to confine their electrons and produce quantum effects. This is a key parameter for naked-eye colorimetric sensing applications, because modifications of their surface charge are transformed into a visible color change. Furthermore, NPs also have a very high extinction coefficient that depends mainly on their size,shape and inter-particle distance. Such properties enable them to compete with analytical techniques, like absorbance or fluorescence spectroscopy. Colorimetric-based assays have been developed by exploiting the color changes associated with the aggregation of metal-noble NPs [2]. Due to their adaptability, high sensitivity, low cost and versatility (Figure 1), AgNP- and AuNP-based assays have been used for the detection of metal ions [3], small molecules [3b, 3f, 4], proteins [3f, 4z, 5], deoxyribonucleic acidDNA [3f, 5i, 6] and enzymes [5a, 6g, 7]. AuNPs are often used as sensing

elements to develop sensitive, selective, simple and label-free colorimetric assays [7h, 8]. Consequently, NP used as detection agents could be considered as a sort of "litmus test" for target molecules [5i, 9].

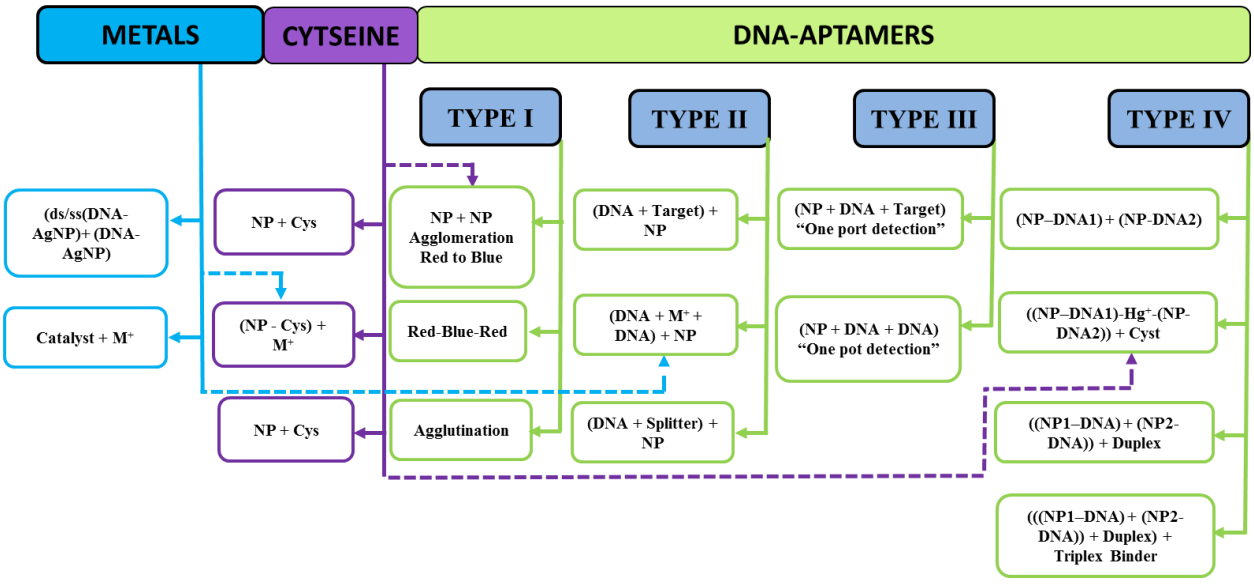

Figure 1: Possible colorimetric detection approaches for metals, ligands and macromolecules.

Although analytical methods, such as high-performance liquid chromatography, electrophoresis, voltammetry and fluorescence spectroscopy, are the preferred approaches for the detection of various macromolecules, sensitive, fast and high-throughput screening methods are still required [4x]. NP-based colorimetric methods are quick and user-friendly detection approaches that take advantage of various chemical mechanisms. For instance, such methods can be used for the rapid detection of influenza viruses through the binding between the influenza virus envelope protein hemagglutinin and sialic acid-stabilized AuNPs [10], or for high-throughput screening of endonuclease inhibitors [7e].

In this review, the colorimetric approaches that allows for the naked-eye detection of color changes through ultraviolet-visible (UV-Vis) absorption spectroscopy without fluorescence detection methods are addressed. Specifically, aptamer-based applications for the detection of metal ions, small ligands and biological macromolecules will be described. Accordingly, the methods have been subdivided on the analytes and the NP's surface modifications and not on the basis of the used NPs, as the colorimetric performances of AgNPs or AuNPs are very similar. The applications involving aqueous/water-soluble stabilized NPs with no solid surface arrays, such as glass will be highlighted. To ensure that all key possibilities are fully explored, the

different sections herein have been divided as follows: detection of metals, small molecule (cysteine, dopamine) and oligonucleotides (cross-linking).

2. Gold and Silver NP synthesis, morphology and properties

The most commonly used methods for the synthesis of AgNPs and AuNPs involve reducing AgCl or $AgNO_3$ and $HAuCl_4$ with sodium citrate and sodium borohydride. The AuNP mixture is boiled with vigorous stirring in a round bottom flask fitted with a reflux condenser for approximately 10 min. Color change from yellow to wine red is observed within a few seconds [4s, 4z, 11]. The AuNP solution concentration can be calculated following Beer's law, using the extinction coefficient of 2.7×10^8 M^{-1} cm^{-1} at λ=520 nm [12]. For AgNPs, 1% tri-sodium citrate is added to 0.3 mM silver nitrate solution, and the mixture stirred for 5 min. After a drop-by-drop addition of 1 mM sodium borohydride solution in the dark, the resulting mixture is stirred at room temperature for 2 h. The bright yellow AgNPs are then filtered through a Millipore syringe (0.45 nm) to remove the precipitate [4t]. NPs are then characterized by diffusion light scattering (DLS) to calculate their hydrodynamic radius in solution, or by transmission electron microscopy (TEM) to describe their morphology (Fig. 2).

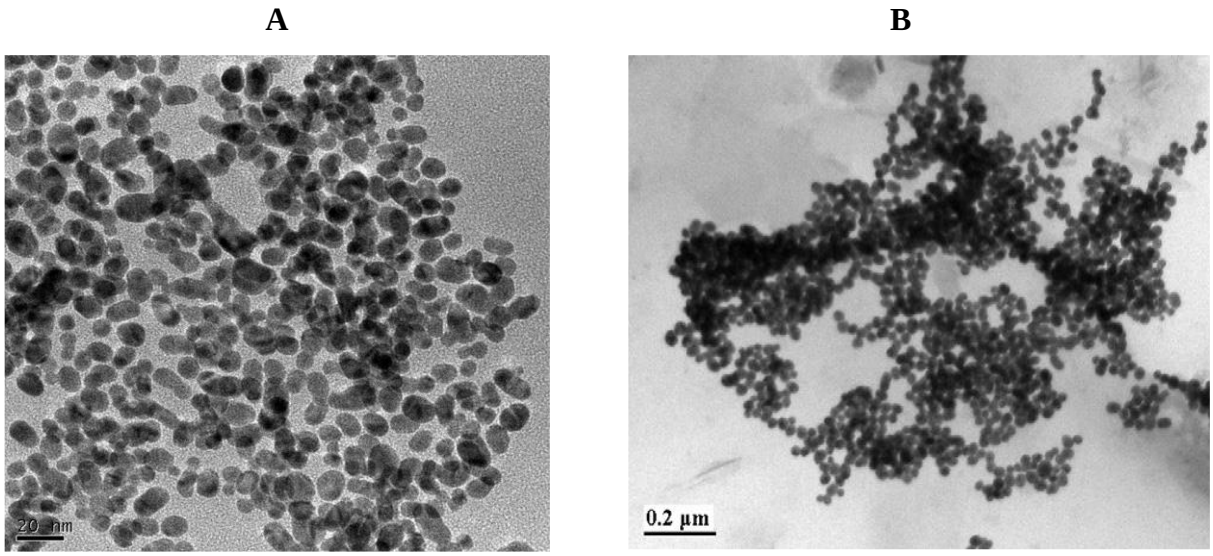

Fig. 2. TEM images of (A) 13 nm citrate-capped AuNPs from wine-red solution [4s] and of (B) guanine-induced AgNP aggregates [13].

For colorimetric assays, AgNPs have some advantages compared with AuNPs. Specifically, AgNP extinction coefficients are higher than those of AuNPs of the same average size [7h], but with AuNPs being more popular. This could be explained by the fact that AgNPs functionalization usually leads to their chemical degradation and thereafter the AgNP surface can be easily oxidized, thus reducing their stability [4f, 7h, 14]. Indeed, Manuco *et al.* reported that AuNPs are stable for more than 1 month at room temperature, whereas AgNPs only for about two weeks. This difference could be linked to the different reaction constants of thiolated gold and silver [15]. The high extinction coefficients and distance-dependent optical properties of AuNPs accounts for the high sensitivity of AuNP-based colorimetric assays. Moreover, color changes can be easily observed by the naked eye, thus making them attractive for DNA-related colorimetric assays [4c, 4k, 6b, 7h, 8]. The DNA adsorption kinetics by AgNPs are slower than those by AuNPs and they cannot be accelerated by adding salt at neutral pH. This unique property of the specific molecular recognition of DNA-related colorimetric assays accounts for the difficulty of attaching DNA to AgNPs at neutral pH [16].

Similarly, AgNPs are good candidates as optical sensors because they display distance-dependent optical properties [4f, 17]. Their stability can be improved by producing Ag/Au core-shell NPs that retains the Ag core optical properties. However, oligonucleotide-modified Ag/Au alloy particles are not as stable as oligonucleotide-modified core-shell particles and irreversibly

aggregate in comparable conditions [17b]. Furthermore, nanoparticles, such as nanorods, prisms, bipyramid of materials, have different SPR wavelengths [15]. For this reason, sensing platforms based on AuNPs optical properties in combination with the molecular recognition of ligands, such as alkyl thiols, antibodies, nucleic acids, and proteins, are active areas of research [3d]. Mirkin's group developed aptamer-based colorimetric assays for macromolecules using the more stable AuNPs, despite AgNPs having a greater extinction coefficient [6c, 18].

NP colloidal stability can be adjusted by modifying the surface charges that affects electrostatic stabilization, and NP aggregation can be induced through loss (or screening) of surface charges. Basically, when AgNPs and AuNPs are exposed to light, they oscillate the electromagnetic field of light. This induces a collective coherent oscillation of conduction band electrons, giving rise to SPR. The SPR band intensity and wavelength depend on the factors that affect the electron charge density on the particle surface. According to Mie's theory, these factors include the metal type, particle size, shape, structure, composition and dielectric constant of the surrounding medium [19]. Thus, unmodified AuNPs are red while AgNPs are blue or maroon due to their specific and size-dependent SPR absorption. Addition of salt triggers electrostatic repulsion between negatively-charged NPs and antiparticle changes, resulting in NPs aggregation and, consequently, specific color and wavelength changes [3e, 4t, 6a, 13]. Hence, by monitoring the changes in absorbance, it is possible to understand the characteristics of the enhanced scattering effect in aggregated NPs compared with non-aggregated NPs [10]. Consequently, the band gap energies can also be used to improve the knowledge on NPs sensing and catalytic properties [20]. The SPR profile is characteristic of the NP surface modification by small molecules, metal ions and bio-macromolecules [21].

3. Detection of metals ions (aggregation induced by interparticle cross-linking)

AgNPs and AuNPs colorimetric changes are due to the particle surface modification and aggregation. This can be achieved by NPs aggregation induced by interparticle bond formation (cross-linking aggregation) or by modifying colloidal stabilization (non-crosslinking aggregation) [7a, 22]. In the non-crosslinking system, aggregation is driven by the London/van der Waals attractive forces between NPs [7a]. Therefore, the presence of specific functional groups, such as hydroxyl (–OH), carboxyl (–COOH) and amine ($–NH_2$), on the NPs surface plays a

critical role in aggregation. By modulating the strength of the NPs intermolecular ion and surface chemistry, this method can be improved [23]. For example, highly charged nucleotides or uncharged nucleosides can bind to citrate-capped AuNPs with the displacement of weakly bound citrate ions through metal–ligand interactions. This can increase AuNPs stabilization or trigger their aggregation, respectively, through gain or loss of surface charges [7a].

Table 1: Detection of metal ions

Nanoparticle	Analyte	Sample/intereferent	Functionalization	Analytical performance	Ref
AuNPs	Mercury Hg^{2+}	River water and tap water	Citrate-AuNPs + 2, 2'-bipyridyl (Bipy)	LOD: 38 nM LDR: 0.2 to 2.0 μM	[24]
AuNPs (20 nm)	Mercury Hg^{2+}	Target-doped blood serum	AuNPs and conjugated polyelectrolyte	LOD: 50 μM	[3f]
AuNPs (12 nm)	H_2O_2	Interferent solutions at different concentration	Citrate-AuNPs	LOD: 1.3 μM LDR: 1.3 to 41 μM	[4a]
AuNPs (17±2 nm)	Cr^{3+}	Tap water and underground water	Mercaptosuccinic acid-AuNPs	LOD: 0.6 μM LDR: 0.6 to 1.4 μM	[11a]
AuNPs (13 nm)	Ag^{+}	Bimetallic conjugate mixtures	Au–PolyT and Ag–PolyA	LODs: 86.8 nM	[14]
AuNPs (13 nm)	Pb^{2+}	Divalent metal ions	DNAzyme–AuNPs	LOD: 0.1 to 4 μM	[3a]
AuNPs (13 nm)	Pb^{2+}	RNA-cleaving DNA enzyme	Aptamer–AuNPs	LDR: 0.020 to 200 μM LODs: 10 μM	[7i]
AuNPs (10 nm)	Pb^{2+}, Pd^{2+}, Hg^{2+}, Pt^{2+}	Standard solutions	Peptide-AuNPs	LODs: nM/ppb range	[3d]
AuNPs (3.5 nm)	K^{+}	Monovalent cations (Li^{+}, Na^{+}, Rb^{+}, NH^{4+}) and bivalent (Ca^{2+} and Mg^{2+})	Aptamer–AuNPs	LOD: 1.0 mM	[3e]
AuNPs (13 nm)	SCN^{-}: thiocyanate	Tap water and common ions	Citrate-AuNPs	LOD: 140 nM	[4s]
AgNPs (9.5±2.0 nm)	Ca^{2+}	Serum and artificial cerebrospinal fluid	AgNPs and cysteine	LOD: 0.1 mM	[4t]

LDR, linear dynamic range; LOD, limit of detection.

Recently, colorimetric measurements based on metal-induced aggregation of small molecules (for instance, cysteine, dopamine), peptides and DNA-functionalized NPs have

160 received considerable attention [3b, 3c, 4i, 11c]. Indeed, aggregation results in changes in the inter-
161 particle distances, leading to a shift of the SPR absorption band of AgNPs to a longer wavelength
162 [4t]. These cross-linking aggregation-based approaches have been used for the detection of metal
163 ions (Table 1). Farhadi *et al*. described the development of a sensitive and selective colorimetric
164 assay based on the interaction between cysteine, sodium dodecyl sulfate (SDS)-capped AgNPs
165 and calcium ions. In the presence of calcium ions and NaCl, AgNPs aggregation was induced,
166 leading to a yellow-to-red color change [3c] (Fig. 3). Mukherjee and co-workers used a similar
167 approach for cysteine detection with AgNPs in the presence of Cr^{3+} [3b]. As in the case for
168 colorimetric assays in which a ligand is used for complexation, these approaches ultimately are
169 effective for detection of both ligands and metal ions. For instance, in the presence of Cu^{2+},
170 ascorbic acid rapidly induces AuNPs aggregation as a result of the Cu^{+}-catalyzed 1,3-dipolar
171 cyclo-addition of azides and alkynes (click reaction). Thus, the AuNPs solution color changed
172 and this was observed by naked eye for LOD of 3 nM [4i].
173

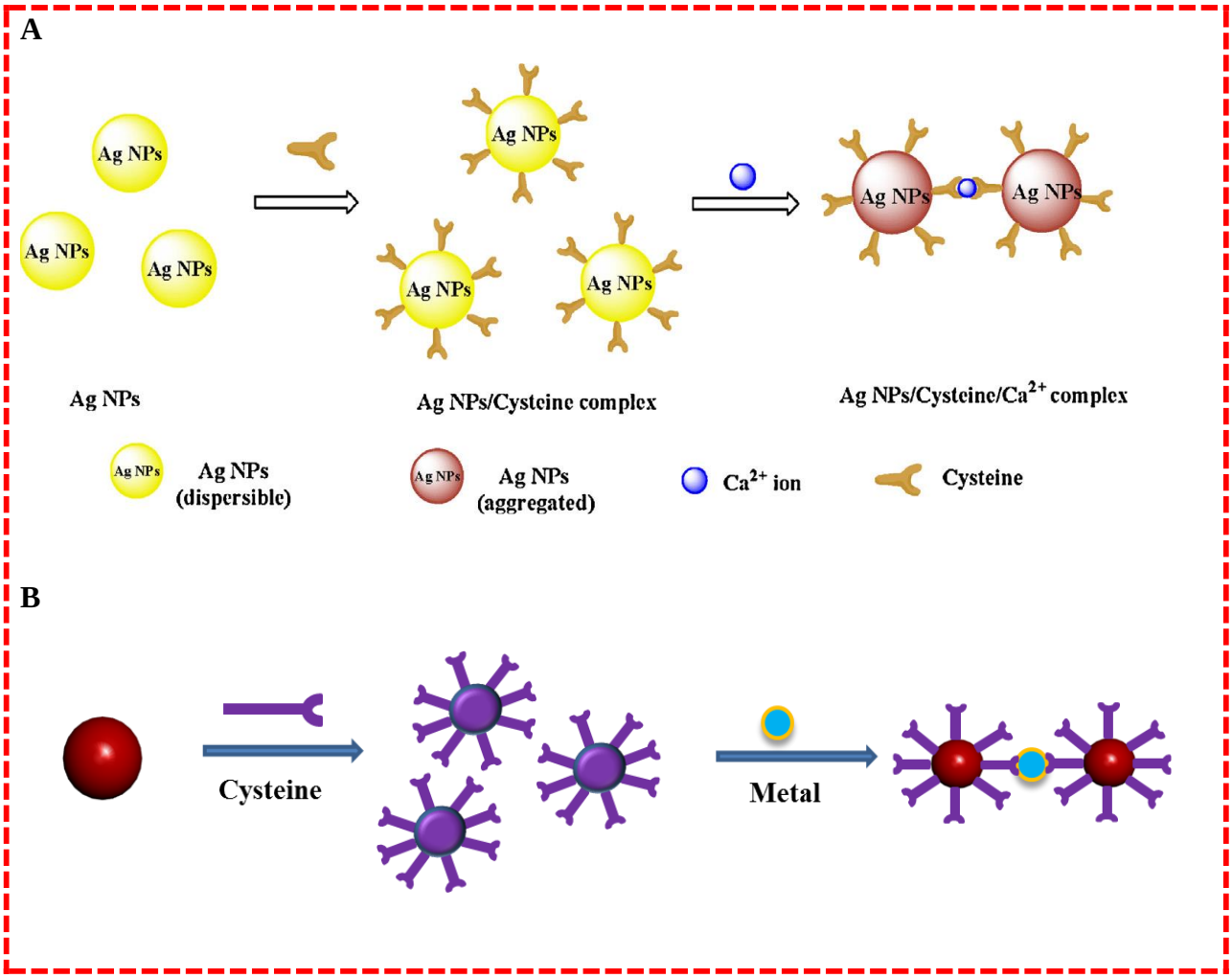

Fig. 3. Schematic illustration of the strategy for cysteine detection using (A) AgNPs and (B) AuNPs. The simultaneous presence of cysteine molecules and Ca^{2+} ions that act as a "glue" to link two neighboring NP-cysteine complexes results in NP cross-linking. Reproduced with permission from [3c].

Enzymes, such as deoxyribozymes (DNAzymes) with high specificity for metal ions ~~and~~ can form blue aggregates with AuNPs, have also been used for the detection of metal ions. Specifically, Pb^{2+} induces NPs aggregation, thus maintaining the color of the original solution [3a].

Peptide-based AuNPs also have been used as colorimetric sensors for metal ions. For example, in the Flg-A3 fusion peptide, the N-terminal Flg (-Asp-Tyr-Lys-Asp-Asp-Asp-Asp-Lys-) includes charged and aromatic residues involved in metal ion complexation, whereas the

A3 peptide (-Ala-Tyr-Ser-Ser-Gly-Pro-Ala-Pro-Pro-Met-Pro-Pro-Phe-) binds to gold surfaces. This led to an overall negative charge (pI=3.9) that prevents NPs aggregation by repulsive forces [3d]. Interestingly, after addition into the solution of peptide-AuNPs, the colorimetric response of each metal ion (Co^{2+}, Hg^{2+}, Pb^{2+}, Pd^{4+} and Pt^{2+}) was different and reproducible and occurs within 1 min [3d] (Fig. 4).

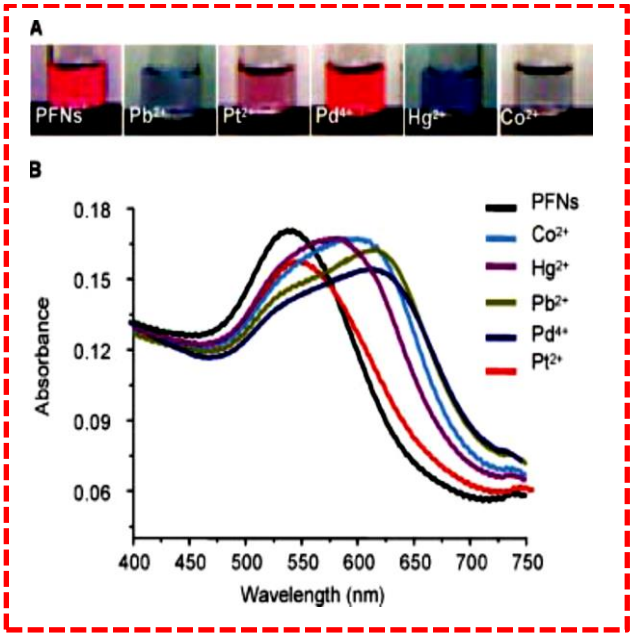

Fig. 4. Colorimetric response of peptide-AuNPs to metal ions. A) Optical microscopy images of peptide-AuNP solutions (10 mM in Au atoms) after exposure to 10mM of different metal salts. B) Corresponding UV/Vis spectra of peptide-AuNPs in the presence of the different metal ions [3d]. PFNs, peptide-AuNPs without metal ions.

This indicates that peptides are versatile ligands and their complexation with metal ions is driven through interaction of the peptide backbone with their amino acid side chains. Modifications in the peptide sequences could affect the metal speciation and coordination geometry [3a, 3d]. The limitation of the peptide-NP colorimetric sensor is that DNAzyme activity in the presence of NPs solution should be minimal.

4. Detection of small molecules: cysteine, dopamine

This section focuses on small molecules such as analytes and colorimetric substrates (Table 2), particularly cysteine and dopamine, because they have been extensively studied.

209 **Table 2: Biomolecule-sensing based on AuNPs or AgNPs aggregation.**

Nanoparticle (size)	Analyte/s	Sample/s	Functionalization	Analytical performance	Ref
AuNPs Monodisperse	Bisphenol-A	Urine and water samples	Aptamer–AuNPs	LOD: 0.01 pg mL^{-1} LDR: 10 000 to 0.1 pg mL^{-1}	[4ab]
AuNPs (40–50 nm) Monodisperse	Concanavalin A	Lectin (jack beans)	Thioglucose-AuNPs	LOD: 9 nM LDR: 10–100 nM (R^2 = 0.983)	[25]
AuNPs (12.33 nm) Monodisperse	Maltose, mannose, glucose, lactose and D-mannopentaose	Carbohydrate-AuNPs	Carbohydrate–protein interactions	NR	[26]
AuNPs (15, 20, and 2.5 nm) Monodisperse	Cysteine, glutathione and glutathione disulfide	Blood/serum	Citrate-AuNPs: 15 nm CTAB-AuNPs: 20 nm $NaBH_4$-coated AuNPs: 2.5 nm	LDR: cysteine, NR LDR: glutathione: 10–100 and 200–800 µM LDR: glutathione disulfide 10–300 and 400–800 µM LOD: cysteine <0.5 LOD: glutathione 10 µM LOD: glutathione disulfide 10 µM	[11b]
AuNPs (~13 nm) Monodisperse	Dopamine	Interferent: ascorbic acid	AuNPs induced by copper ions	LOD: 30 nM LDR 1: 33 nM to 100 nM LDR 2: 0.1 µM to 4.5 µM	[4i]
AuNPs (15 nm) Monodisperse	Dopamine (DA)	Spiked serum	DA inhibits melamine-induced AuNP aggregation	LOD: 33 nM LDR: 33 nM to 3.33 mM	[12]
AuNPs (13 nm) Monodisperse	Dopamine	Common interferents, such as 3,4-dihydroxyphenylalanine (DOPA), catechol, 3,4-dihydroxyphenylacetic acid (DOPAC), homovanillic acid (HVA), epinephrine (EP) and ascorbic acid (AA).	The aptamer conformational change could facilitate salt-induced AuNP aggregation 58-mer dopamine-binding aptamer (DBA)	LOD: 360 nM LDR: 0.54 -5.4 µM	[27]

AuNPs ±15 nm Multi-dispersed	Dopamine (DA)	Human urine, human serum	DA-induced aggregation of 4-amino-3-hydrazino-5-mercapto-1,2,4-triazol (AHMT) –AuNPs through hydrogen-bonding interactions	LOD: 70 nM LDR: 0.2–1.1 μM	[28]
AuNPs Monodisperse	Dopamine (DA)	Human serum	DA colorimetric sensing based on AuNP aggregation induced by copper ions	LOD: 200 nM LDR: 0.5–10 μM	[29]
AgNPs (NR) Monodisperse	Coralyne	Selectivity test against intercalating ligands, ethidium bromide (EB) and daunomycin (DM)	Homoadenine-AgNPs, label-free colorimetric detection of small molecules using DNA oligonucleotides and AgNPs	LOD: 0.25 coralyne molecules/adenine base	[4f]
AgNPs (5–15 nm) Multi-disperse	4-nitroaniline (4-NA)	self-assembled AgNPs on DNA	4-NA reduction to para-phenylenediamine		[20]
AgNPs (12 ± 2 nm) Multi-disperse	Adenine, guanine, cytosine, thymine	NR	Strength of interactions between the fundamental chemical components of DNA and AgNP surfaces	NR	[13]
AuNPs (13 nm) Multi-disperse	Ampicillin	ssDNA aptamer-AuNPs	Colorimetric assay of ampicillin using specific aptamers	LOD: 5 ng mL^{-1}	[4l]
AuNPs	Oxytetracycline	Tetracyclines (TCs) as counter targets	Ultrasensitive colorimetric detection of oxytetracycline using shortened aptamer	LOD: 0.1 nM	[4v]
AuNPs (13 nm)	Oxytetracycline	Aptamer-AuNPs	Aptamer-specific colorimetric assay	LOD: 25 nM LDR: 25 nM to 1 μM	[4g]
AuNPs (18 nm) Monodisperse	Bisphenol a	Water samples	AuNP aggregation by competitive binding of bisphenol A and aptamer	LOD: 0.1 $ngmL^{-1}$	[4q]
AuNPs (13 nm) Multi-disperse	Ochratoxin A	Standards	Aggregation occurs as random coil structures to compact rigid antiparallel G-quadruplexes	LDR: 20 to 625 nM LOD: 20 nM	[4k]
AuNPs (13 nm) Monodisperse	Cysteine	Amino acids, glutathione, thioglycolic acid and mercaptoethyl alcohol	2:1 cysteine/Cu^{2+} complex	LOD: 10 nM	[11c]
AuNPs (13 nm) Monodisperse	Ascorbic acid	Fruit juices	Alkyne–azide click reaction	LOD: 3.0 nM	[4i]

AuNPs (NR) Monodisperse	Cysteine	19 amino acids	ssDNA-AuNPs	LOD: 100 nM LDR: 0.1 to 5 μM	[4e]
AuNPs (20.1±1.8 nm) Multi-disperse	Influenza B/Victoria, influenza B/Yamagata	Virus dilution (hemagglutination assay titer, 512)	Sialic acid-AuNPs	LOD: 0.09 vol%. upper limit of linearity 2.5 vol %	[10]
AuNPs (13 nm) Monodisperse	Tryptophan enantiomers	D/L enantiomers	AuNPs	LOD: 0.1 μM	[4y]
AuNPs (~11.89 nm) Mono-disperse	Arginine, histidine, lysine	Urine samples	Quercetin-AuNPs	LOD: 0.04, 0.03, and 0.02 μM. LDR: 2.5–1,250 μM (Arg) and 1–1,000 μM (His and Lys),	[30]
AuNPs-I (15 nm) AuNPs-II (30 nm) AuNPs-III (40 nm) Multi-disperse	Melamine	Pre-treated milk	Citrate-AuNPs	AuNPs-I (2.37 x10^{-8} M) AuNPs-II (3.3 x 10^{-8} M) AuNPs-III (8.9 x 10^{-8} M)	[4z]
AgNPs (NR) Mono-disperse	Cysteine	Various metals	2:1 cysteine/Ca^{2+} complex	LOD: 83 nM LDR: 0.25 – 10 μM	[3c]
AgNPs (10 – 15 nm) Multi-disperse	Cysteine	10 mM of nine amino acids	2:1 cysteine/Cr^{3+} complex	LOD: 1 nM	[3b]
AgNPs (10-20 nm) Multi-disperse	Dopamine, L-DOPA, noradrenaline adrenaline	Tyrosinase	AgNPs	LOD: dopamine, L-DOPA and noradrenaline 2.5 μM adrenaline 20 μM tyrosinase activity~10 units (~100 μg mL^{-1})	[4b]
AuNPs (~ 13 nm) Multi-disperse	Kanamycin	Other antibiotics: streptomycin, sulfadimethoxine and ampicillin	ssDNA aptamer-AuNPs	LOD: 10 nM	[4j]
AuNPs (~ 13 nm) Mono-disperse	Sulfadimethoxine (SDM)	NR	AuNPs	LDR: 50 ng mL^{-1} to 1.0 μg mL^{-1} LOD: 50 ng mL^{-1}	[4n]
AuNPs (~15 nm)	Penicillin G	Different penicillins	CTAB-AuNPs	LOD: 0.007 mg mL^{-1}	[7m]

Multi-disperse					
AuNPs (20 nm) Mono-disperse	Cysteine	19 essential amino acids	DNA-AuNPs	LOD: 100 nM LDR: 100 nM – 2 µM	[4d]
AuNPs (13 nm) Multi-disperse	Adenosine	inosine, guanosine, and cytosine	aptamer-OD-AuNPs	LOD: 10 µM	[31]
AuNPs (13 nm) Mono-disperse	Adenosine and caffeine	Other nucleosides	Aptamers	LOD: 0.3 mM	[4c]
AuNPs (15 nm) Mono-disperse	Digitoxin	Rat serum	AuNPs	LOD: 571 pM	[4aa]
AuNPs (10.8-13.1 nm) Multi-disperse	Cysteine	Interferents: Na^{+}, Cu^{2+}, Cl^{+} and urea	AuNPs	LDR: 0.1 to 0.6 ppm LOD: 0.01ppm	[4u]
AgNPs (5 – 20 nm) Multi-disperse	Cysteine/cystine	Other amino acids	AgNPs	LDR: 25–250 µM LOD: 2.5 ppm	[4m]
AgNPs (8 nm) Mono-disperse	Cysteine and homocysteine	Human urine and plasma samples	Non-ionic fluorosurfactant-AuNPs,	LOD: 0.4 µM.	[4o]
AgNPs (8±1.6nm) Multi-disperse	Cysteine	Human urine and plasma samples	Fluorosurfactant-AgNPs	LOD: 0.05 µM. LDR: 1.5–6.0 µM	[4r]
AgNPs (9.5±2.0 nm) Multi-disperse	Cysteine	Serum and artificial cerebrospinal fluid	AgNPs and Ca^{2+}	LDR: 0.1–1000 µM LOD: 0.1 µM	[4t]
AuNPs (20.0±1.4) nm Multi-disperse	Cysteine	Human urine	Pectinase-protected AuNPs	LDR: $4.85x10^{-6}$ to 302 µM and 3.25 to 0.103 mM LOD: $4.6x10^{-9}$ M.	[4ac]
AuNPs (13 nm) Monodisperse	Cysteine	Brain microdialysate (sample), lactate, ascorbic acid and glucose (interferents)	Cysteine-AuNPs	LDR: 0.166 to 1.67 µM LOD: 0.1 µM	[23]
AuNPs (13 nm) Monodisperse	Pyruvic acid	Interferents: lactic acid (LA), ascorbic acid (AA) and glucose.	AuNPs	LDR: 5.6 µM to 168.0 µM LOD: 3.0 µM	[4w]
AuNPs (13 nm) Monodisperse	Sulfadimethoxine (SDM), kanamycin (KAN) and adenosine	Mixture of KAN, SDM and ADE	Aptamer of KAN, SDM and ADE (1:1:1 mixture).	NR	[4x]

	(ADE)				
AuNPs (13 nm) Monodisperse	17β-estradiol	Intereferents: methanol, diethylstilbestrol, bisphenol A, 19-nortestosterone, estroil, estrone	AuNPs	LOD: 0.1 ng mL^{-1}	[4x]
AuNPs (20 nm) Monodisperse	Caffeine	ATP and target-doped blood serum	AuNPs	LOD: 1.25 μM	[3f]
AuNPs (13 nm) Monodisperse	Parathion	Sea and tap water	Parathion inhibits AChE-induced aggregation of AuNPs	LDR: 15 to 65 ppb and 140 to 1000 ppb LOD: 0.7 ppb (2.4 nM)	[4ad]

CTAB: cetyl trimethyl ammonium bromide; OD: oligonucleotides; SDM: sulfadimethoxine; KAN: kanamycin; ADE: adenosine; AChE: acetylcholinesterase, Cyt C: cytochrome c.; LDR: linear dynamic range; LOD: limit of detection.

Cysteine has been employed as a common strategy for the detection of metals, but it also can be quantified by colorimetric assays. Metal ions are used as cross-linking agents for cysteine-AuNP or –AgNP pairs to induce NP aggregation and the consequent red to blue color change of the NP solution is observed. The degree of aggregation depends on the cysteine concentration and the average AuNPs diameter in the presence of different cysteine concentrations. In such colorimetric assays, organic molecules bind to the Au/AgNPs surface via their amine ($-NH_2$) (blue) or thiol (−SH) (yellow) terminal groups (Fig 5).

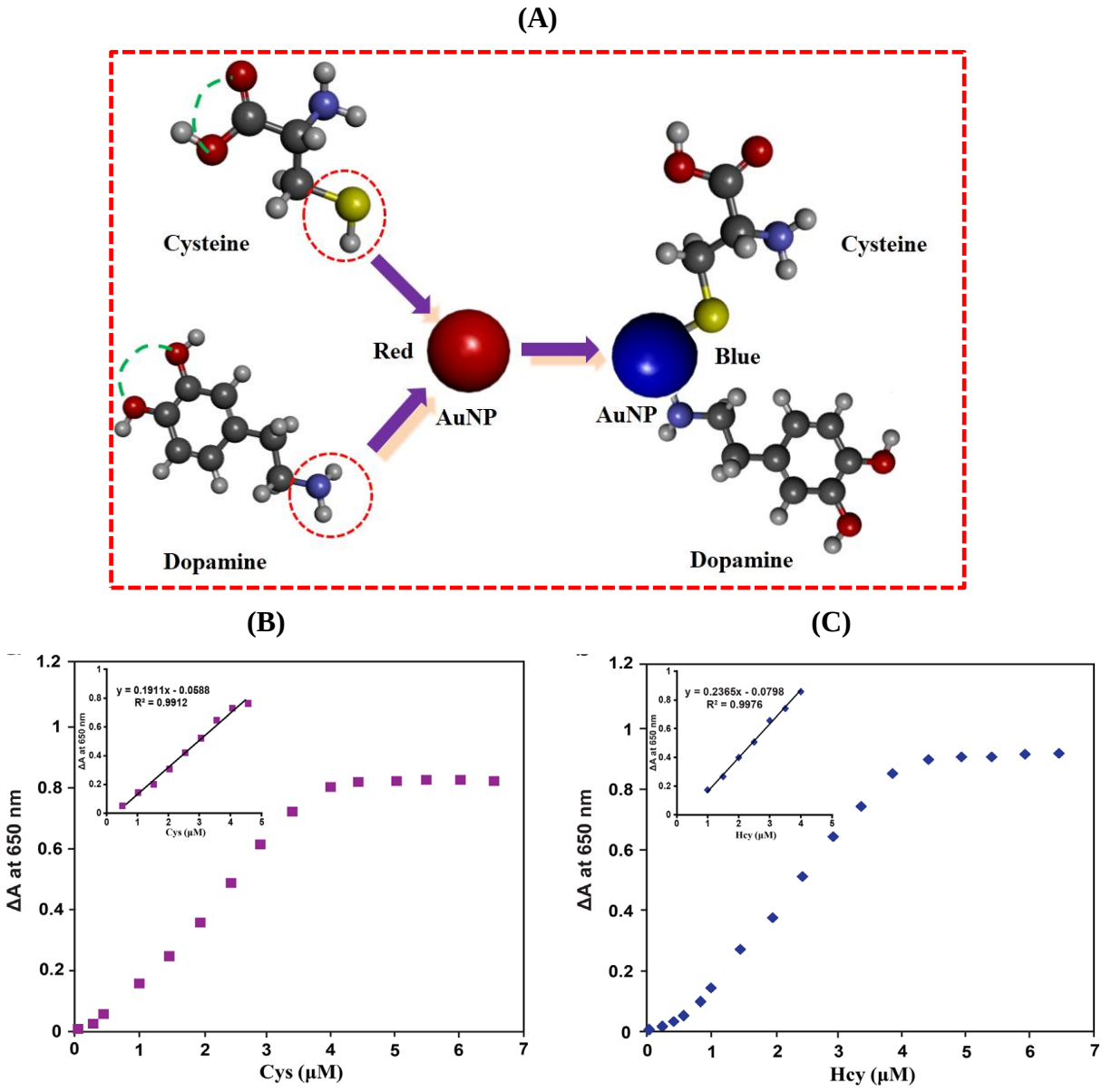

Fig. 5A) Chemisorption model for cysteine and dopamine on the AuNP surface. The solution color changes from red to blue in the presence of cysteine or dopamine. B and C shows linear relationship of nonionic fluorosurfactant-capped gold nanoparticles versus Cys and Hcy 650 nm. The linear range for Cys was 0.5–4.5 μM, and for Hcy was 1.0–4.0 μM. Conditions: pH 6.5, 100 mM NaCl , 30 s incubation period at 50 ºC

Ligands with the $C_6H_8O_6$ formula, without $-NH_2$ or $-SH$ functional groups, preferably bind to the AuNPs surface, and are highly unlikely to induce AuNPs aggregation [4i, 4u, 32].

The thiol groups of cysteine interact with the surface of colloidal AuNPs or AgNPs via chemisorption-type interactions; however, cysteine can complex with metal ions, such as Pb^{2+}, Zn^{2+}, Cu^{2+} [4i, 11c], Ca^{2+} [3c, 4t], Cr^{3+} [3b], at a ratio of two cysteines for each metal ion [10, 11c]. In the presence of metal ions, cysteines can induce AgNP and AuNP aggregation with a color change from yellow to purple and blue to red, respectively [3b, 3c, 4u, 11c]. These assays are based on the NP distance-dependent optical properties after coordination, as confirmed by the change in the zeta potential from -30.7 mV for pure AgNPs to -19.63 mV after interaction with cysteine and Cr^{3+} [3b]. Specifically, Hajizadeh *et al.* reported that cysteine can rapidly induce AgNP aggregation (yellow-to-red color change) in the presence of Ca^{2+} and 10 mM NaCl, leading to a decrease in electrostatic repulsion and faster aggregation [3c]. Cysteine concentration can be determined also by using AuNPs and a UV-Vis spectrometer with a LOD of 10 nM (1.2 ng ml^{-1}) [11c]. The ratio between absorption at 524 and absorption at 396 nm (A_{524}/A_{396}) is linear with a cysteine concentration range from 0.25 to 10 mM (R^2 = 0.993) with a LOD of 83 nM [3c]. Jongjinakool and co-workers detected cysteine in a concentration range from 0.1 to 0.6 ppm with a LOD of 0.01 ppm [4u]. In Figure 5b-c, a multi-component mixtures demonstrated that cysteine and homocysteine were identified based on the different SPR wavelengths induced by aggregation of non-ionic fluoro-surfactant-functionalized AuNPs upon addition of a mixture of the amino acids. The absorbance changes due to AuNPs aggregation induced by cysteine and homocysteine increase the individual absorbance values (LDR from 0.5 to 4.5 μM for cysteine and LOD (S/N=3) of 0.4 μM for homocysteine) [4o].

When dopamine (DA) and Cu^{2+} solutions are mixed, the amine group directly coordinates with Cu^{2+} without nitrogen atoms bonded to the gold surface [4i]. The LOD for DA is 30 nM with, differently from cysteine-based methods, a linear calibration curve for two concentration ranges (3.3×10^{-8} to 1.0×10^{-7} M and 3.0×10^{-7} to 4.5×10^{-6} M) with correlation coefficients of 0.9981 and 0.9979, respectively [4i]. Likewise, addition of 5 mM Cu^{2+} improves

the colorimetric probe to a LOD of 200 nM [29]. AuNPs also can be used for the quantitative colorimetric detection of neurotransmitters that mediate the generation and growth of AuNPs, with a LOD of 2.5 μM for dopamine, L-DOPA and noradrenaline, and of 20 μM for adrenaline [4b]. The metal ion-Au/AgNPs interaction is mainly a coulombic interaction and its strength is directly related to the molecular structure and charged groups. Therefore, selectivity can be improved by working on these two parameters [4r]. For instance, researchers highlighted the excellent selectivity of AuNP-based colorimetric assays for cysteine compared with other biomolecules, such as thioglycolic acid and mercaptoethyl alcohol [11c], glutathione [11b, 11c] glutathione disulfide [11b], aspartic acid and glutamic acid [23]. Moreover, selectivity changes also when using cysteine derivatives, namely glycine, dipeptide Cys-Gly, cysteamine, mercaptopropionic acid, S-protected (S-methyl-L-cysteine), N-protected (N-acetylcysteine) and O-protected cysteine (L-cysteine methylester hydrochloride), as indicated by the color change from yellow to pink and peak broadening [4m]. Therefore, it is imperative to investigate the detection of sulfur-containing amino acids compared with other standard amino acids [4m]. Chen *et al.* used 19 naturally occurring amino acids, but they could not improve the colorimetric response of cysteine [4e].

Another strategy for cysteine detection is based on the observation that when cysteine is added to AuNPs/ssDNA, the ssDNA molecules that stabilize AuNPs against salt-induced aggregation are displayed spontaneously by cysteine encapsulation on the AuNPs surfaces, via an Au–S bond [4e]. The salt-induced aggregations result in a characteristic AuNPs color change from red to blue [4e, 4m]. According to Chen *et al.* [4e] this approach is not feasible with other amino acids (Fig 6).

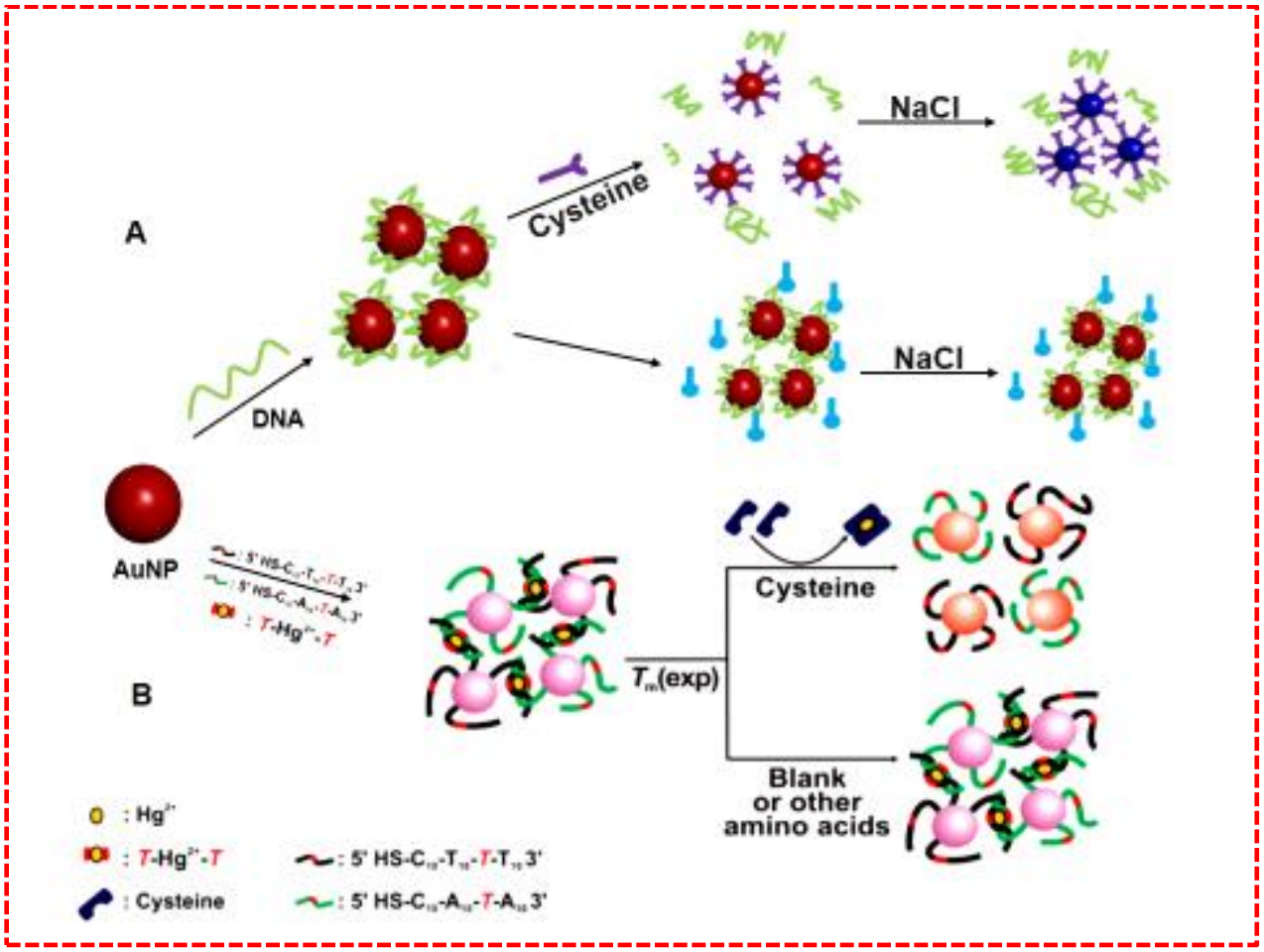

Fig. 6. In the presence of cysteine, the ssDNAs is displayed **by cysteine on AuNPs surface resulting in AuNP aggregation and in a color change from red to blue upon addition of NaCl. Other amino acids do not lead to a color change due to the absence of thiol groups [4e]. (B) Cysteine colorimetric detection using AuNPs probes that contain T-T mismatches complexed with Hg^{2+}: competitive approach in which cysteine can displace Hg^{2+}[4d]**

In this system, the A_{640}/A_{525} ratio is linearly dependent on the cysteine concentration (from 0.1 to 5.0 μM with LOD of 100 nM) [4e]. Differently from methods that require AuNPs modification, this approach is simple and fast, but it requires specific links between the biomolecules and AuNPs to allow ssDNA displacement from the NPs surface. On the other hand, Mirkin's group developed a cysteine detection assay where two sets of AuNPs probes are functionalized with different oligonucleotide sequences (probe **A**: 5' HS-C10-A10-**T**-A10 3'; probe **B**: 5' HS-C10-T10-**T**-T10 3') and rapidly form aggregates upon combination through the thymidine-thymidine (T-T) mismatches complexed with Hg^{2+} with LODs as low as a 100 nM [4d]. Comparison of the two methods (ssDNA-AuNPs and mismatch assay) highlights that they rely on the distance-dependent optical properties of AuNPs, the sharp melting transition of oligonucleotide-AuNPs

aggregates and the very selective coordination of Hg^{2+} with cysteine during which the purple-to-red color change occurs [4d, 4e]. However proteins with one free cysteine residue, such as human serum albumin, can spontaneously attach to AuNPs surfaces through Au-S bond formation [2]. These studies demonstrate that the presence of negatively-charged carboxyl groups in the cross-linkers remains essential to induce AuNPs aggregation through ion pair interactions between amino groups present in cysteines and carboxyl groups in the cross-linkers [4m, 23]. On comparison of the dopamine- and cysteine-based methods it was evident that functional groups present on the surface also plays a key role in metal detection.

4.1. Recognition of chiral molecules

Stereochemistry plays a central role in molecular recognition and interactions. Indeed, the molecule's chemical and biological properties depends not only on the nature of their constituent atoms, but also on their position in space [32b]. Currently, chiral molecules are mostly separated with techniques like capillary electrophoresis, high-performance liquid and gas chromatography. Nanoparticles allow for the easy detection of chiral molecules by the naked eye. For instance, the color of the AuNPs solution changes from red to blue in the presence of D-tryptophan (LOD of 0.1 μM and LDR of 0.2–10 μM), but not of L-tryptophan [4y]. Interestingly, AuNPs can selectively adsorb D-tryptophan, and therefore, L-tryptophan molecules can easily be separated by simple centrifugation of the tryptophan/AuNP solution [4y]. The infrared spectra confirms the D-tryptophan absorption to AuNPs by disappearance of the NH (NH^{3+}) stretching absorption peaks (3078 and 3038 cm^{-1}), leaving the carboxylic group (-COOH) and nitrogen atom of the indole ring free for further coordination. This distinctive feature allows for binding of one Cu^{2+} ion to two tryptophan molecules by coordination with the COOH and nitrogen atom of the indole ring, hence allowing for recognition [4y]. Another reported visual differentiation is between the D- and L-forms of mandelic acid (MA) was based on their chirality towards 13 nm l-tartaric acid-capped AuNPs. The L-MA solution changes the red colour of l-TA-capped AuNPs to a bare-eye observable blue, while d-MA does not trigger any color changes [33]. The AgNPs capped with a novel chiral R-mandelic acid-derived calix[4]arene (R-MAC4), for it good optical and structural properties. These self-assembled NPs were used to recognize the N-Fmoc-d/l-aspartic acid (d/l-FAA)[34].

4.2. Detection of macromolecules

Nanoparticles can be easily modified by replacing surface-adsorbed weak ligands (e.g., negatively charged citrate ions) with thiolated macromolecules that are difficult to displace due to their strong binding to the surface.

Xue and co-workers described citrate-AuNP-based assays for trypsin and arginine residues screening (Fig. 8). The aggregation of negatively charged citrate-capped AuNPs in the presence of a peptide composed of six arginine residues (Arg_6) occurred mainly through electrostatic interactions, and led to a red-shift of the usual SPR profile [35]. However, when the Arg_6 peptide was hydrolyzed into fragments upon trypsin addition in the solution, the

electrostatic interactions between AuNPs and arginine residues were weakened and, therefore, neither AuNPs aggregation nor SPR shift was observed.

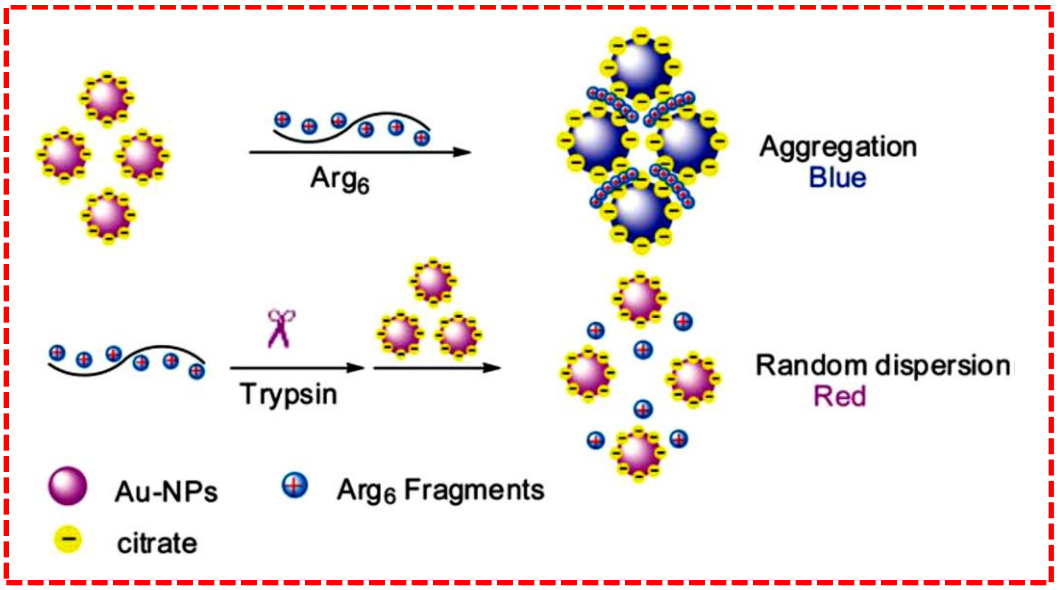

Fig. 7. Colorimetric assay for trypsin by using AuNP crosslinking/aggregation based on trypsin-catalyzed hydrolysis of Arg_6 for random dispersion of citrate capped AuNPs. Reproduced with permission from [35].

Moreover, Arg_6 hydrolysis catalyzed by trypsin is retarded if trypsin inhibitors are present in the solution. This feature was used to develop a label-free assay for trypsin (LOD: 1.6 ng ml^{-1}) and Arg_6 residues screening with AuNPs [35]. Similarly, interaction of citrate-AuNPs with fibrinogen to form fibrinogen–AuNPs through electrostatic and hydrophobic interactions was used for the detection of thrombin (LOD: 0.04 pM and LDR: 0.1–10 pM; R^2 = 0.96) [7l]. Although the mechanism of detection was the same, the molecular interactions was different. Indeed, fibrinogen was adsorbed on NPs before the addition of thrombin [7l]. Conversely, trypsin interacts with Arg_6 before the NPs addition into the system [35]. Detection of thrombin has been improved by the use of catalytic enlargement as shown in Fig. 9. [5a].

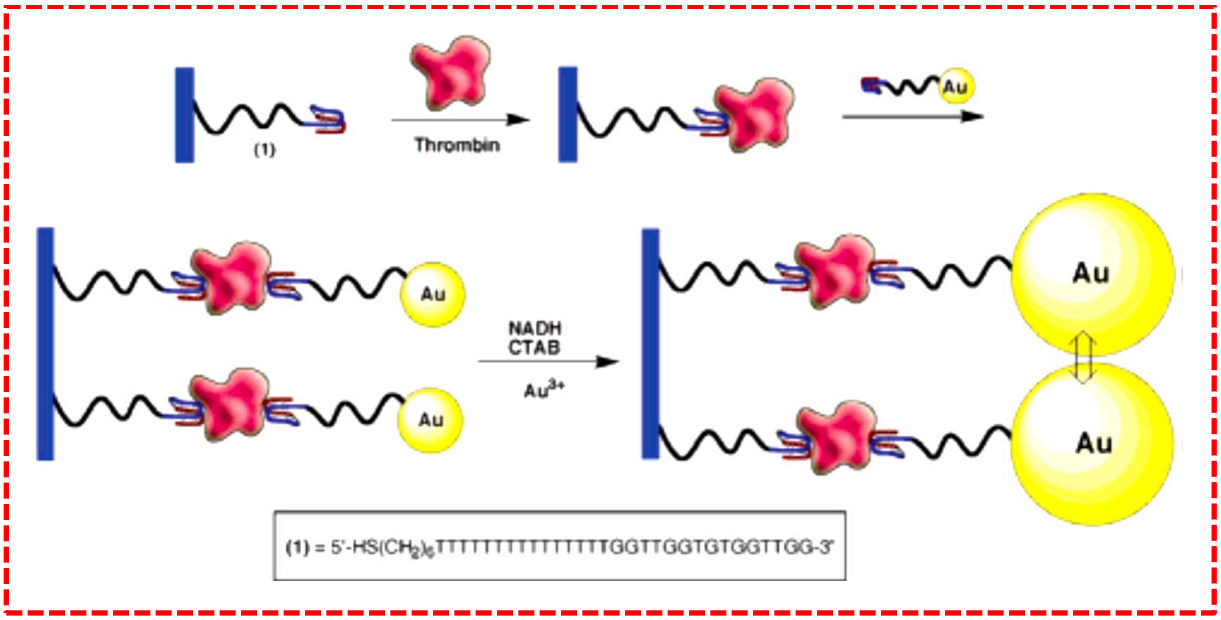

Fig. 8. Amplified thrombin detection on surfaces by catalytic enlargement of thrombin-aptamer-functionalized Au-NPs [5a]. As the concentration of thrombin increases, the surface loading of bound thrombin is higher, resulting in a number of Au NP seeds for enlargement.

Specifically, upon aptamer-AuNPs reaction with thrombin, AuNPs aggregate. But in the presence of other proteins (200 nM BSA or human IgG antibodies), the aptamer-AuNPs does not precipitate implying that the precipitation originates from the specific interaction between aptamer and thrombin (LOD: 20 nM) [5a].

Similarly, Chen's group evaluated the possibility of using mannopyranoside-encapsulated AuNPs/concanavalin (Man-AuNPs/Con A) complexes for a competitive colorimetric assay for ten proteins. However, only thyroglobulin, *bandeiraea simplicifolia* lectin I (BS-I), soybean agglutinin (SBA) and *maackia amurensis* (MAL) significantly modified the absorption spectrum of Man-AuNPs/Con A complexes [5b]. In contrast to the method proposed by Xue *et al.* [35], where upon the introduction of thrombin in the fibrin–AuNP solutions, catalyzes the polymerization of the free and conjugated fibrinogen species to form insoluble fibrillar fibrin–AuNP agglutinates [7l]. Finally, Guarise *et al.* exploited the fact that, compared with the native peptide substrates, protease-cleaved peptides do not induce NPs aggregation (and thus the color of the solution does not change) to detect two proteases (thrombin and lethal factor) [36].

Quercetin-AuNPs have been used as a colorimetric probe for the detection of amino acids, such as arginine (Arg), histidine (His) and lysine (Lys). Indeed, quercetin-AuNPs aggregation caused by amino acids leads to a color change from red to blue [30]. In optimal

conditions, a linear relationship exists between the absorption ratios at different wavelengths (A_{702}/A_{525} for Arg, A_{693}/A_{525} for His, and A_{745}/A_{525} nm for Lys) and the concentration ranges (from 1.25 to 2.50 μM for Arg; from 1 to 1,00 μM for His and Lys), with LOD values of 0.04, 0.03, and 0.02 μM, respectively, at pH 5.0 [30]. Siddhartha and Debabrata reported that protein estimation is within a LOD of 10-80 μg mL^{-1} using unmodified AgNPs [5h].

Lately, the sequence-length-dependent adsorption of ssDNA on AuNPs has been investigated for colorimetric nuclease assays and measurement of oxidative DNA damage [6g]. Based on ssDNA adsorption rate on citrate-AuNPs, it can be hypothesized that incubation with AuNPs for a specific period of time can lead to differential adsorption of short and long ssDNA. Consequently, the stability of the ssDNA-AuNPs complex in the presence of salt could be influenced by the ssDNA length [6g]. The confirmation of this hypothesis led to the development of colorimetric assays taking advantage of ssDNA length to improve adsorption. For example, when ssDNA is cleaved by the S1 nuclease or –OH radicals in small fragments, these shorter ssDNA can be rapidly adsorbed on AuNPs and significantly enhance the negative charge density on each AuNP surface for the same time of incubation (Fig. 9).

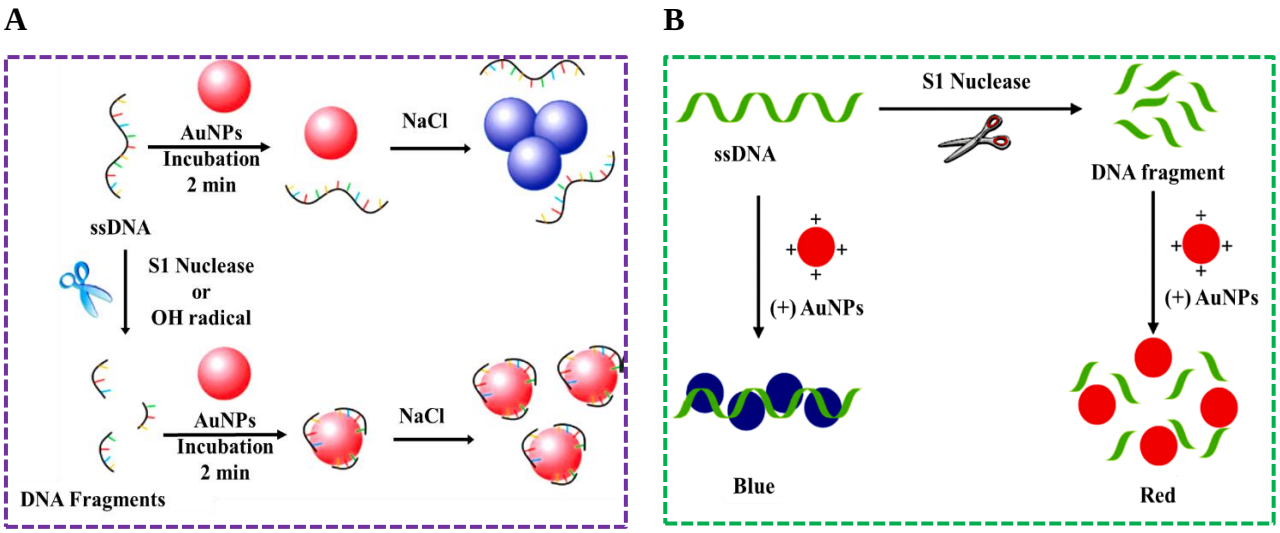

Fig. 9. Schematic representation of AuNP-based colorimetric strategies for ssDNA cleavage assays. (a) Salt-induced NP aggregation before and after ssDNA cleavage by the S1 nuclease or OH radicals. Reproduced with permission from [6g]. (b) Nuclease activity assay using positively charged AuNPs and polyanionic ssDNA ((+)AuNPs). Reproduced with permission from [7n].

Basically, charging the NPs surface increases the electrostatic repulsion between the ssDNA-AuNPs complexes enough to inhibit NP aggregation at the same salt concentration, and the solution color does not change. Thus, DNA cleavage can be directly visualized by naked eye [6g].

Charge interaction between positively charged AuNPs and polyanionic ssDNA leads to AuNPs aggregation that can be monitored by the color change from red to blue (Fig. 9) [7n]. However, in the presence of the S1 nuclease, the ssDNA substrate is cleaved into small fragments, and the AuNPs solution remains red. Thus, the nuclease activity can be easily monitored by naked eye or with a simple colorimetric reader [7n]. In this case, the exocyclic amino group of nucleotides is the main cause of nucleotide-dependent aggregation because cysteamine-capped AuNPs are positively-charged at pH 3.6 (with a pKa of 10.75), leading to efficient electrostatic interactions with the negatively charged DNA. These results complement each other because during S1 enzymatic activity, ssDNA is degraded into smaller fragments that cannot induce aggregation [6g, 7n].

Additionally, the non-crosslinking AuNPs aggregation induced by the loss of surface charges also is exploited for enzymatic activity testing and screening for potential inhibitors [7a]. This approach has been extended to the serotype I-specific detection of dengue virus DNA. In the absence of the DNA target solution, peptide nucleic acids (PNA) induce AuNPs aggregation with a red-to-purple color change and the appearance of a second absorbance peak at 650 nm due to the AuNPs surface coating by PNA [37]. Likewise, sialic acid-reduced and -stabilized AuNPs (d= 20.17 ± 1.8 nm) can be used for the colorimetric detection of influenza viruses [10]. The discrimination of such molecules can also be standardized using chemometric techniques including hierarchical cluster analysis and principal component analysis. This approah was used to accurately classified and measure the array response of cysteine, gluthatione, glutathione disulfide and interferences without any misclassification [38].

5. DNA-functionalized nanoparticles (aptasensors)

This is the most fascinating area of NP-based colorimetric assays. Much attention has been focused on aptamers (i.e., ssDNAs and oligopeptides with high binding affinity and selectivity for target molecules) as powerful biological macromolecules (Table 3). Particularly, the aptamer advantages compared with antibodies, such as possibility of chemical synthesis and modification and lower immunogenic response, contribute to their potential [4j]. They are generally selected *in vitro* by using the systematic evolution of ligands by exponential enrichment (SELEX) technique and random-sequence nucleic acid libraries [4j, 4l, 4p, 4v, 4x, 39]. This allows selecting, the highest binding aptamer(s). Then, aptamers can be capped with thiol groups that bind to two AuNPs [6c, 9, 18]. The principle of colorimetric sensing based on aptamers to detect specific DNA sequences was introduced about a decade ago and is now a key tool in biodiagnostics [9, 18]. Since then, other aptamer-based sensors have been developed for the detection of metal ions, small molecules [4d, 4e] and proteins [5c, 5g, 7d].

Table 3: DNA/protein sensing based on AuNP aggregation

Nanoparticle (size)	Analyte/Target	Functionalization	Analytical application	Analytical performance	Ref.
AuNPs (13 nm) and AgNPs (10 -20 nm) Monodisperse	DNA3 complementary DNA	DNA1-AuNPs DNA2-AgNPs	Complementary DNA recognition	NR	[16]
AuNPs (12.33 nm) Monodisperse	Maltose > mannose > glucose > lactose > MAN5.	Carbohydrates-AuNPs	carbohydrate–lectin interactions	NR	[26]
AuNPs (13-nm) Monodisperse	Lysozyme	HSA-AuNPs	Colorimetric detection	LOD: 50 nM.	[7f]
AgNPs (10-15 nm) Monodisperse	Globular proteins (BSA and IgG)	AgNPs	Concentration-dependent particle agglutination	LOD: 10 to 80 μg mL^{-1}	[5h]
AuNPs and AgNPs Monodisperse	Specific DNA sequence	AuNPs and AgNPs	Detection of DNA through nucleic acids (PNA) hybridization	LOD: DNA/PNA ratio of 0.05	[6a]
AuNPs (50 nm) Multidisperse	Con A	p-Aminophenyl-D-mannose- AuNPs	Carbohydrate–lectin system	LOD: 9.0 nM (R^2 = 0.983) LDR: 10-100 nM	[25]
AuNPs Multidisperse	PDGFs and PDGFR	Apt-AuNPs	Protein analysis and cancer diagnosis	-2.5-10 and 10-20 nM, respectively, for 0.42 nM Apt-	[5c]

				AuNPs -25-75 and 75-200 nM, respectively, for 8.4 nM Apt-AuNPs.	
AuNPs (32 nm) Monodisperse	Con A binding partners	Mannopyranoside-encapsulated gold nanoparticles (Man-AuNPs)	Competitive colorimetric assay for ConA binding partners through protein–protein interactions	NR	[5b]
AuNPs (13 nm) Monodisperse	24-bp polynucleotide target	AuNPs capped with 3¢- and 5¢ (alkanethiol) oligonucleotides	Hybridization of the target with the probes		[6c]
AuNPs (20 nm) Monodisperse	H_2N-Cys-Tyr(PO_3^{2-})-Arg-OH	AuNPs	Sensing phosphatase activity of alkaline phosphatase	54: 3.4 uM of peptide : alkaline phosphate	[40]
AuNPs (15 nm) Monodisperse	Bla molecules	AuNPs	β-Lactamase activity Identification of Bla molecules and screening for Bla inhibitors	60 pM	[41]
AgNPs (31 nm) Multidisperse	AgNP-oligonucleotide conjugates	DNA-AgNPs	Hybridization of two complementary DNA-AgNPs	NR	[17a]
AuNPs (13 nm) Monodisperse	Single-stranded DNA cleavage	AuNPs	Enzymatic cleavage and oxidative damage of single-stranded DNA	NR	[6g]
AuNPs (14 nm) Monodisperse	HIV-1 ribonuclease H	AuNPs	Colorimetric detection of HIV-1 ribonuclease H activity by AuNPs	27 units mL^{-1}	[7o]
AuNPs (13 nm) Monodisperse	Tyrosin	AuNPs	Crosslinking/ aggregation of Au-NPs based on trypsin-catalyzed hydrolysis of Arg6	1.6 ng mL^{-1}	[35]
AuNPs Monodisperse	Methyltransferase activity	DNA-AuNPs	Colorimetric assay for endonuclease/ methyltransferase activity and inhibition	NR	[7k]
AuNPs (13 nm) Monodisperse		DNA-modified AuNPs	Enzymatic cleavage of nucleic acids, colorimetric biosensors	0.5 units mL^{-1}	[7i]
AuNPs (13 nm) Monodisperse	Thrombin	Aptamer-AuNPs	Colorimetric assay based on the aptamer folding and unfolding	LDR: 0 to 167 nM LOD: 0.83 nM	[5g]
AuNPs (20 nm) Monodisperse	Thrombin	AuNPs	G-quadruplex structure folding	LOD: 10 nM	[3f]
AuNPs (NR)	Triplex DNA binders: BePI or CORA	Aptamer-AuNPs	Screening triplex DNA binders	NR	[42]

AuNPs (13.3±1.2 nm) Multidisperse	Thrombin	Fibrinogen-AuNPs (56 nm)	Colorimetric assay for blood plasma	LOD: 0.04 pM LDR: 0.1 to 10 pM	[7l]
AgNPs (NR) Multidisperse	CIAP and PKA	AgNPs	Adenosine phosphorylation and dephosphorylation	LOD: CIAP: 1.0 unit mL^{-1} PKA: 0.022 unit mL^{-1}	[7h]
AuNPs (~ 12.74 nm) Monodisperse	staphylococcal enterotoxin B	AuNPs	Colorimetric assay based on aggregation in the absence of the aptamer	LDR: 10 to 50 ng mL^{-1} LOD : 10 ng mL^{-1}	[4p]
AuNPs (NR) Multidisperse	Aminopeptidase N	Gold nano-composites conjugated with a thermo-responsive copolymer	Activity based on inhibition of the disassembly of Gold nano-composites	AR: 20 to 50 U L^{-1}	[43]
AuNPs (15.1 nm) Multidisperse	β-galactosidase and β-glucosidase	Gal-Lip-AuNPs and Glc-Lip-AuNPs	Glycosidase inhibitor screening	LODs: β-galactosidase 9.2 nM and β-glucosidase 22.3 nM at 20°C	[44]
AuNPs (26 nm) Monodisperse	ADA	AuNPs	Nucleotide-dependent aggregation	LOD: 0.8227 U L^{-1}	[8]
AuNPs (13 nm) Monodisperse	Endonuclease	DNA-AuNPs with duplex interconnection	Endonuclease activity and inhibition	NR	[7e]
AuNPs (13 nm) Monodisperse	Biotin (biotinylation)	Peptide-AuNPs and avidin-AuNPs	Kinase-catalyzed substrate biotinylation	NR	[7d]
AuNPs (20 nm) Multidisperse	Protein kinase A,	AuNPs	Kinase activity based on the coagulating ability of a cationic substrate peptide and its phosphorylation	NR	[7g]
AuNPs (NR) Multidisperse	Acetylcholinesterase	Citrate-AuNPs	AChE-catalyzed hydrolysis of acetylthiocholine	0.6 mU mL^{-1}	[45]
AuNPs (16 nm) AgNPs (16 nm) Monodisperse	Con A	Mannose AuNPs Mannose-AgNPs	Con A induced aggregation	Mannose -AuNPs LOD: 0.04 µM LDR: 0.04-0.10 µM Mannose-AgNPs: LDR: 0.08 – 0.26 µM LOD: 0.1µM	[2]

AuNPs (15 nm) AgNPs (20 nm) Monodisperse	Kaposi's sarcoma associated herpesvirus and Bartonella DNA	Oligonunucleotides-AuNPs Oligonunucleotides-AgNPs	Aggregation reaction with multi-color changes	LOD: 1 nM	[15]
AgNPs (10-15 nm) Multidisperse	BSA and immunoglobulins	AgNPs	Nanoparticle agglutination	LOD: 10 -80 μg mL^{-1}	[5h]
AuNPs (21 nm) Monodisperse	polyA, polyC, polyU, polyI, BSA, lysozyme, dsDNA,ssDNA	AuNPs	Aggregation due to self-assembly (discrimination and detection)	LOD: Protein ~100 pM Homopolynuclotide ~10 pM	[5i]
AuNPs (13.2 nm) Monodisperse	Dengue virus	AuNPs	PNA/DNA hybridization	LOD: 0.12 μM	[37]
AuNPs (~13 nm) Monodisperse	ssDNA and dsDNA	AuNPs	DNA sequences based on electrostatic interactions	AR: 100 fmol	[6e]
AuNPs (13 nm) Monodisperse	Abrin	Catalytic AuNPs	Peroxidase-like activity	LDR: 0.2 to 17.5 nM LOD: 0.05 nM	[46]
AuNPs (13 nm) Monodisperse	Lipase	Tween 20-GNPs	Enzyme-regulated AuNP aggregation	LOD: 0.028 mg mL^{-1} LDR: 0.15 to 1.80 mg mL^{-1}	[7p]
AuNPs (50 nm) Multidisperse	Native proteins	DNA-AuNPs	50% human urine	Cluster analysis	[5j]

NR: Not Reported; CIAP: Calf Intestine Alkaline Phosphatase; HSA-AuNPs : Human serum albumin-modified gold nanoparticles, PKA: Protein Kinase A; SEB: Staphylococcal enterotoxin B; LOD: Limit of detection; AR: Activity Range; PDGFs : Platelet-derived growth factors; PDGFR : platelet- derived growth factor receptors,, Con A: Concanavalin A; Man-AuNPs: Mannopyranoside- encapsulated gold nanoparticles; Gal: β-galactosidase and Glc: β-glucosidase; ADA: Adenosine Deaminase; AChE: Acetylcholinesterase, KSHV: Kaposi's sarcoma associated herpesvirus; BePI: benzo[e]pyridoindole; CORA: coralyne, BSA: Bovine serum albumin: PNA: peptide nucleic acid; LDR: linear dynamic range; LOD: limit of detection.

The development of DNA-aptamer-based colorimetric assays by Mirkin's group was inspired by the fact that the steps necessary for NPs+ modification with ligands can be tedious or time-consuming and relatively expensive[6c, 18, 47]. NPs stabilized by ssDNA aptamers do not aggregate with the addition of salt only [3e, 4c]. Conversely, in the presence of the target/analyte, the aptamer is folded because it binds to the target while desorbing from the NPs surface, which leads to NPs aggregation and colorimetric changes. Ideally, folded aptamers or dsDNAs should hardly adsorb onto the NPs. This is related to the higher structure rigidity and high proton density inside

dsDNA [3e, 4g, 4x, 6e]. Indeed, ssDNAs cannot hybridize with each other to form dsDNAs. Thus, their strategy is based on the observation that unmodified AuNPs and AgNPs can differentiate between ssDNA and dsDNA, mainly due to the higher structure rigidity of the latter [3e, 4n, 6e]. However, not only the strands but also their lengths contribute to NP stabilization. For instance, Chen and co-workers tested ssDNAs of different length (18nt: 5′ TAG AAT ACT CCC CCAGGT 3′); 24nt: 5′ GGT TGG TCA GAT TCA GTG GGT TAG 3′, and 30nt: 5′ AAA CCC CCC TGC TAAAAC CCC AAA CCC 3′) for AuNP stabilization and consequently for detection and sensitivity. They found that the longer ssDNAs have a better stabilization effect because at the same molar concentration, longer ssDNAs have more monomeric deoxynucleotide units. Moreover, it is difficult for cysteine to replace highly stable DNA-protected AuNPs [4e]. DNA bases possess higher affinity towards gold than silver via coordination between Au and nitrogen atoms (thus favoring DNA adsorption). However, the negatively charged surfaces of AuNPs electrostatically repel DNA phosphate backbones (reducing DNA adsorption) [3e]. The key challenge to their successful application is in transforming the aptamer-binding events into physically detectable signals [4c].

The development of the nanotechnology for NPs functionalization with DNA and the biotechnology for the *in vitro* selection of target-specific nucleic acids offer a unique opportunity for designing colorimetric biosensors [7c, 17a]. The four types of DNA aptamer-based colorimetric approaches are highlighted below:

5.1. TYPE I: Aptamers adsorbed on nanoparticles

Type I aptasensors includes two common steps: i) adsorption of the DNA unit onto the NPs surface and ii) recognition of the target molecule by the DNA strands while serving as an optical sensing element. DNA adsorption on NPs surface is favored by the high charge density and stability provided by the aptamer [4f] (Fig. 10). This is a crucial step because the selectivity of the targeting molecule must be retained during adsorption onto NPs, especially when the aptamer is designed for qualitative assays [4f]. The aptamer conjugation constant is stronger than that of antibodies and that of non-specific adsorption between aptamer and NPs [4q]. With these conditions in mind, Xu and co-workers used unmodified DNA and AgNPs to detect ligands binding to homoadenine, by monitoring the color change from yellow to brown due to AgNP aggregation after salt addition. When coralyne binds to the homoadenine sequence in the aptamer, the aptamer is removed from the AgNP surface and AgNP can aggregate [4f]. The

A_{550}/A_{397} ratio shows a good linear correlation with coralyne concentrations between 0.0 and 10 mM with a LOD of 0.3 mM [4f]. Using a similar strategy, DNA-AuNPs/AgNPs were used to detect several targets, such as bisphenol A (LOD: 0.1 ng mL^{-1} [4q] and LOD: 0.01 pg mL^{-1} [4ab]), digoxin (LOD: 571 pM) [4aa], oxytetracycline (OTC) (LOD: 25 nM) [4g], thrombin, (LOD: 0.83 nM) [5g], kanamycin (LOD: 25 nM) [4j], OTC (LOD: 0.1 nM), ampicillin (LOD: 5 ng mL^{-1}) [4l], staphylococcal enterotoxin B (LOD: 10 ng ml^{-1}) [4p], and pyruvic acid (LOD: 3.0 μM) [4w].

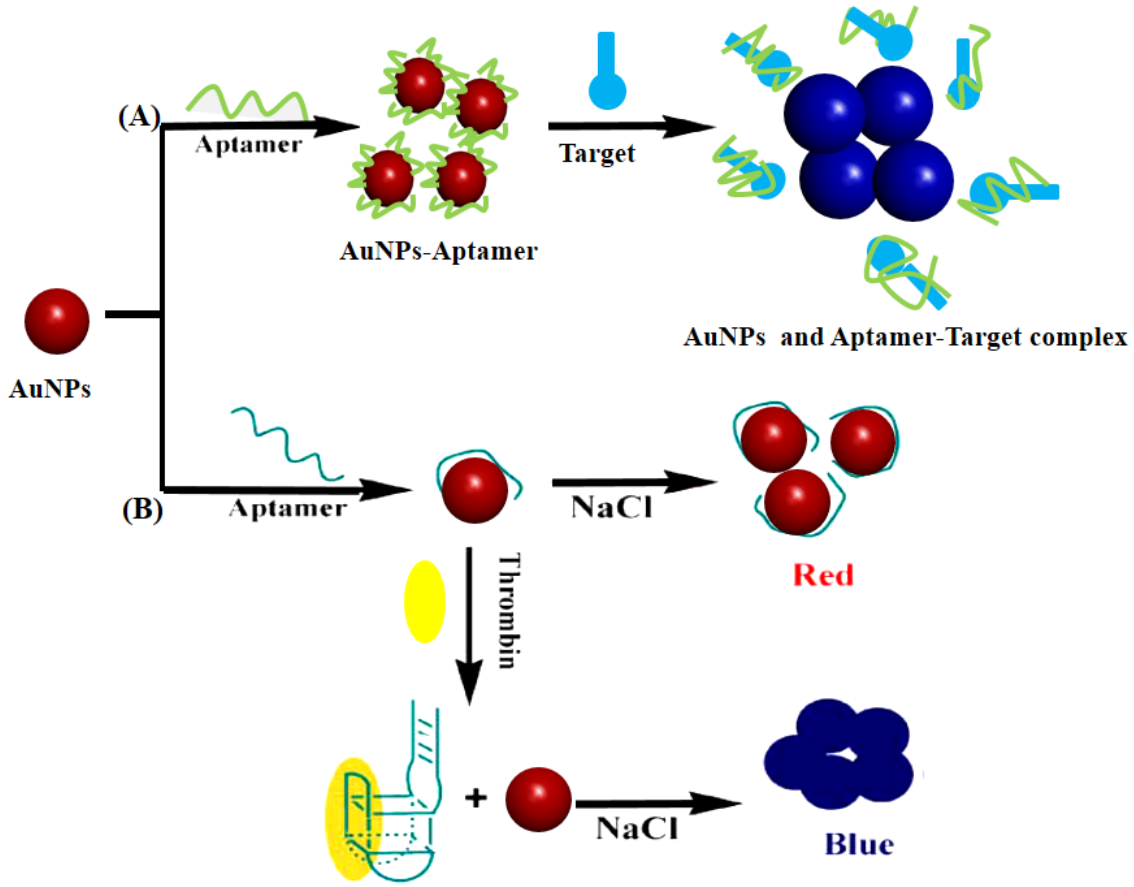

Fig. 10. Schematic representation of Type I colorimetric aptasensors for detection (A) small [4q, 4aa] and (b) large molecular targets [5g]

It is acknowledged that for many type I aptamers, addition of the target/ligand induces the aptamer release from the NP surface and consequently the color change as the salt tolerance decreased by NPs [4f, 4q, 4aa, 48]. Two groups reported an intriguing observation using a similar approach [4c, 49]. When aptamers are added to NPs, their interaction via hybridization leads to NP aggregation and consequently to the color change from red to blue. Addition of the target molecule (e.g., adenosine) to the aptamer-NP solution induces a dramatic conformational change

of the aptamer structure that leads to the dissociation of the NP network and to a new color change (blue to red) [4c, 49].

AuNPs have also been used by Dong's group [5g] to understand the conformational changes of thrombin-binding aptamers (TBA) when they are removed from the AuNP colloidal solution in the presence or not of thrombin. Addition of 100 mL of 0.5 M NaCl causes a quick color change (red to purple) in the solution with thrombin, but not in that with only TBA.. Due to the color change, the TBA conformation modification from unfolded to G-quadruplex/duplex formation could be directly monitored by naked eye, thus allowing the easy detection of thrombin [5g]. Likewise, the addition of enough salt could be used to inhibit the repulsion between unmodified negatively charged AuNPs and result in their aggregation and in the corresponding red-to-blue color change. As previously reported, there is stronger coordination interaction between the nitrogen atoms of unfolded ssDNA and AuNPs than electrostatic repulsion between the negatively charged phosphate backbone and the negatively charged AuNPs [5g]. Conversely, the relatively rigid structure of dsDNA or folded ssDNA (e.g., G-quadruplexes) prevents the exposure of the DNA bases to AuNPs and the high density of negative charges increases the repulsion between DNA and AuNPs. However aggregation of DNA-functionalized AuNPs can be induced also by hybridization of target DNA that does not cross-link the NPs. A conceivable disadvantage of this non-crosslinking system, compared with the crosslinking system, is the consumption of target DNA [48].

Recently, a viable approach to overcome the limitations of type I aptamers due to the DNA length was reported. Briefly, the design of shortened aptamers is mainly based on selecting nucleotide bases characterized by high homogeneity in accordance with their conserved regions [4l, 4v]. Shortened aptamers that contain common regions have approximately the same binding affinity as the original. For instance, based on the conserved sequences with high homogeneity of the original five 76-mer aptamers, A1 and A2 (8-mer sequences) were successfully obtained and still exhibited high affinity and specificity for tetracycline (TC) [4v] (Fig. 11).

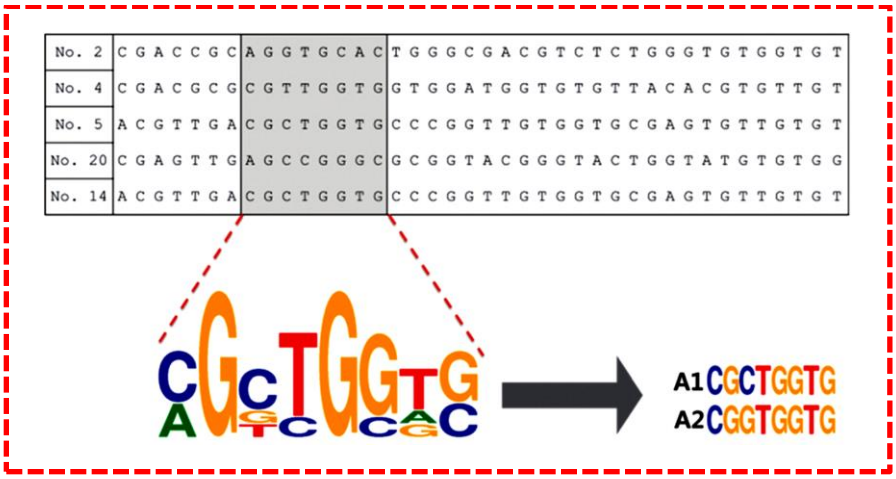

Fig. 11: Truncation process after analysis of the sequences of the original five 76-mer aptamers that bind to oxytetracycline, 20 to 8 mer [4v].

Although only the original stacking pocket and six additional specific bases are present in A1 and A2, they display higher binding affinity (K_d 1.067 nM for TC). The LOD of A2 for oxytetracycline (OTC) was0.1 nM, which is about 500-fold better than that of the original 76-mer aptamer, and the color change can be detected in the presence of 10 nM OTC [4v]. Similarly, based on their common sequence and predicted structure, Changill Ban's group [4l] shortened three 90-mer ssDNA aptamers that specifically bind to ampicillin to obtain AMP4 (21-mer 5′-CACGGCATGGTGGGCGTCGTG-3′), AMP17 (19-mer 5′-GCGGGCGGTTGTATAGCGG-3′), and AMP18 (21-mer 5′ TTAGTTGGGGTTCAGTTGG-3′) [4l]. Comparison of AMP17, AMP4 and AMP18 (at concentrations of 100 mM, 150 mM, and 200 mM, respectively) showed that ampicillin can be detected at concentrations as low as 5 ng mL^{-1} using the AuNP-based dual fluorescence–colorimetric method and in a milk sample at 10 ng mL^{-1} [4l].

Thus, the results by Song *et al.* [4v] and Kwon *et al.* [4l] illustrate and confirm that using aptamers harboring only the binding site/active site sequence can further improve their selective features.

Importantly, the target must not react or crosslink with NPs. Moreover, the ratio between NPs and aptamer could affect the final sensitivity. Too many aptamers in the sensing system reduce the sensitivity, while too few decrease the stability of the sensing systems [4q]. One of the primary challenges of Type I approaches relies on the different binding affinities of ssDNA and dsDNA towards unmodified NPs. However, the important feature is that negatively charged

ssDNA sequences can effectively stabilize NPs against salt-induced aggregation, providing a convenient route for colorimetric assays without NP surface biomodification.

5.2. TYPE II: Aptamer-target adsorbed on nanoparticles

Type II aptamers also include two common steps: (i) aptamer linkage to the target molecule to form a complex, and (ii) aptamer-target complex adsorption to the NP surface. With Type II approaches, it is always wise to check the interaction of the pure aptamer with NPs (Type I) because the system may follow a similar mechanism [4c, 50]. Ideally, aptamer adsorption onto the NP surface should not lead to NP aggregation (and thus color change) after addition of high salt concentration. In the presence of the target, the aptamers should bind in competition with AuNPs, resulting in a color change in the presence of salts. A typical Type II system has been used by Chen *et al.* for sulfadimethoxine (SDM) detection using unmodified AuNPs. In optimal conditions (pH 8, 0.2 mM of aptamer and 2 M of salt), the LDR was 50 ng mL^{-1} to 1 mg mL^{-1} and the LOD was 50 ng mL^{-1} [4n].

Upon addition of SDM, the conformation of the SDM-binding aptamer changes from a random coil structure to a more folded rigid structure that promotes the detachment of the adsorbed aptamers from AuNPs and results in the subsequent AuNP aggregation after salt addition (Fig. 15). This leads to a color change from red to purple-blue that can be easily observed by naked eye [4n]. Recently, Liu *et al.* assessed whether aptamer truncation could improve the sensitivity also in Type II aptamers [4x] (Fig. 1).

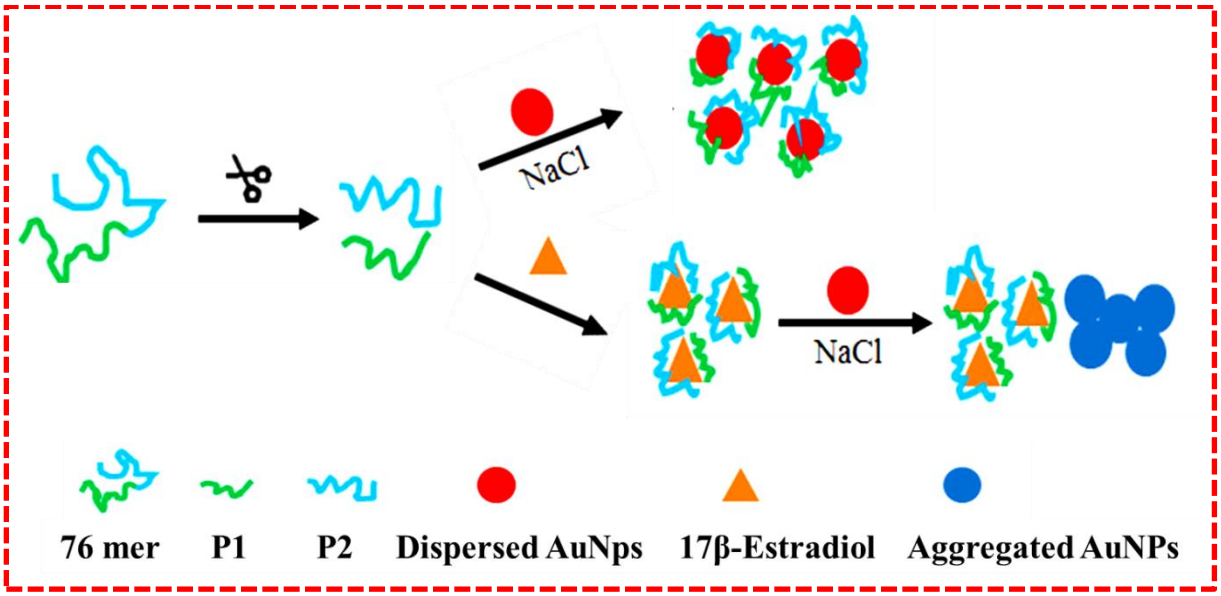

Fig. 12. Schematic illustration of an AuNP-based colorimetric aptasensor to detect 17β-estradiol using split aptamers. Reproduced from [4x]. Split aptamers binds irreversibly to the target analyte

Briefly, the long (76-mer) aptamer specific for 17β-estradiol was split in two shorter sequences (P1 and P2) that still retain the original aptamer affinity and specificity, but with 10-fold higher LODs. Indeed, 17 β-estradiol could be detected with a LDR from 0.1 ng mL^{-1} to 105 ng mL^{-1} [4x]. The authors hypothesized that this increased sensitivity is caused by the lower aptamer adsorption concentration and lower affinity for AuNPs of the shorter ssDNA sequences [4v, 4x]. Likewise, Xie *et al.* developed an assay in which incubation of a RNA-DNA duplex with the HIV-1 reverse transcriptase (RT) leads to the production of ssDNAs and ssRNAs that can form a charged protecting layer on the AuNPs surface and consequently, to NP stabilization at a precisely defined salt concentration (Fig. 17). In the absence of RT, the selected RNA–DNA duplex remains intact, and the unprotected AuNPs aggregate in the presence of salt with a concomitant change in color [7o].

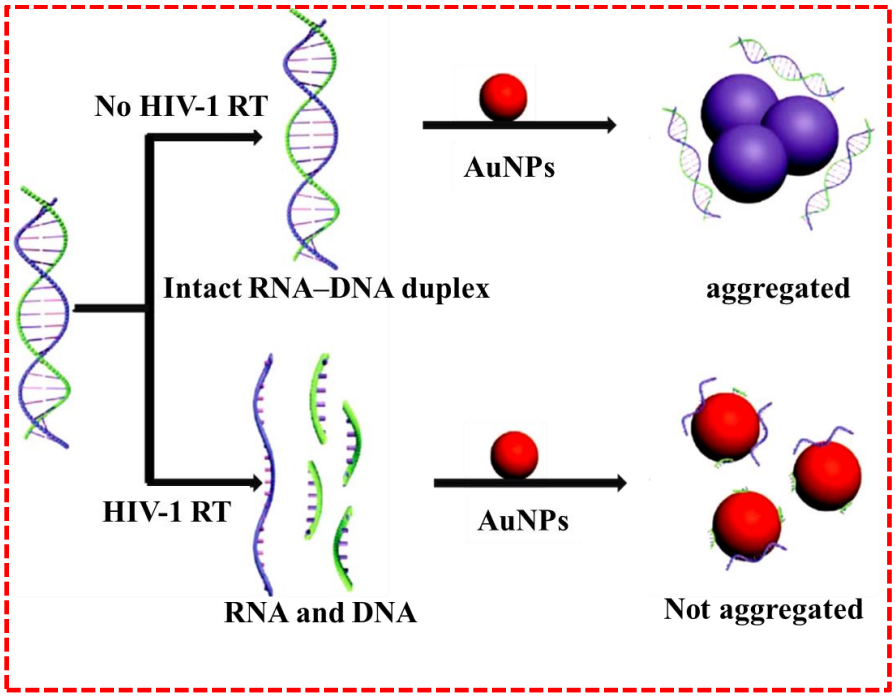

Fig. 13. Schematic of the approach by Xie *et al*. A synthetic RNA–DNA duplex substrate is first incubated or not with HIV-1 RT. HIV-1 RT should cleave the RNA into fragments, resulting in the dissociation of ssDNA and ssRNA probes at room temperature (≈ 28 °C). Reproduced with permission from [7o]. GNPs, AuNPs.

Wang *et. al* [3e] used K^+ as a target because it stabilizes ssDNA, thus facilitating the formation of G-tetrads within 4 min. AuNPs incubated with G-tetrads changes color (red-to-purple) like unmodified AuNPs, suggesting that the G-tetrad structure is not significantly adsorbed onto AuNPs [3e]. The presented assay, which uses C-rich (5'-CCTCCCTCCTTTTCC ACCCACC-3') oligonucleotide aptamers, cationic polymers and AuNPs, provides a platform for the detection of other ions and molecules [3g] (Fig. 18). For instance, in the presence of Ag+, the two oligonucleotide form a tightly bound complex with a C-Ag^+-C notation and change conformation, from a random coil to a hairpin structure with a stronger π-π* transition of the bases with deoxyribose. The resulting C-Ag^+-C complex poorly interacts with a cationic polymer known as Poly (diallyldimethylammonium chloride) (PDDA) and subsequently the polymer aggregates AuNPs through electrostatic interactions, with a color change from wine red to blue [3g]. In the absence of Ag^+, the positively charged polymer can electrostatically interact with ssDNA and destroy the charge balance, leading to induction of AuNP aggregation (LOD of 48.6 nM and LDR from 100 to 1000 nM for Ag^+). Together, the results by Wang *et al.* [3e, 3g] are in

agreement with the hypothesis that unstructured DNA oligonucleotides strongly adsorb onto the NP surface and prevent salt-induced NP aggregation.

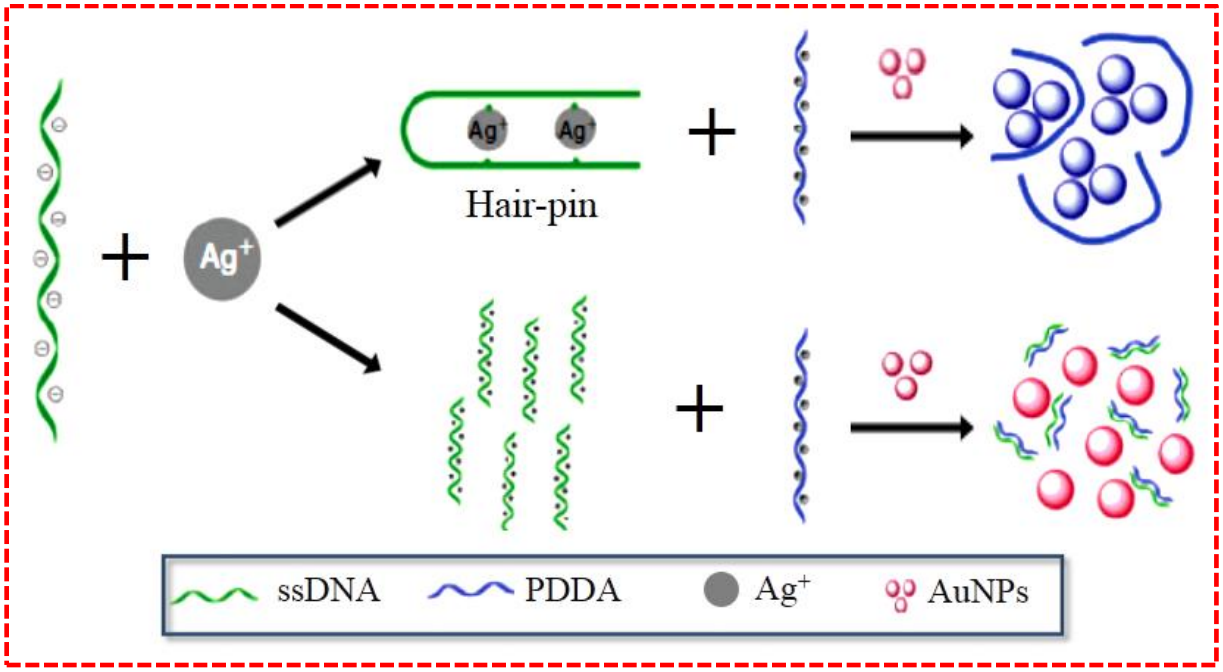

Fig. 14. Schematic description of the colorimetric lead biosensor for Ag^+ detection based on AuNP aggregation induced by PDDA and Ag^+ aptamers [3g].

Recently, Zhang *et al.* [7p] demonstrated that AuNPs possess peroxidase-like activity that can catalyze 3, 3, 5, 5-tetramethylbenzidine (TMB) in the presence of H_2O_2. AuNP peroxidase-like activity can be improved by surface activation with target-specific aptamers. However, by increasing the concentration of abrin (i.e., the target), AuNP peroxidase-like activity decreases and the aptamer is desorbed from the AuNP surface, resulting in a decrease of AuNP catalytic activity. The LDR for the current analytical system ranges from 0.2 nM to 17.5 nM with LOD of 0.05 nM [7p].

Comparison of Type I and Type II systems shows that aptamer-NP complexes are preferentially formed in Type I and aptamer-target complexes in type II systems. It is reasonable to expect less sensitivity from Type I systems because the colorimetric changes are related to the aptamer detachment from the NP surface. The amount of aptamer removed will depend on the amount of target. On the other hand, Type II systems are limited by the fact that the aptamer is expected to retain its adsorption properties after complexation with the target. This suggests that if it is

folded during target binding, it should be flexible enough to facilitate colorimetric changes. Overall it all depends on the aptamer capability because we would prefer induced aggregation in the absence of the aptamer.

5.3. TYPE III: Competition in "One-pot detection systems"

Type III approaches are an intermediate between Type I and Type II systems because the aptamer and the target (or targets) interacts in the presence of NPs, and therefore, this approach is often referred to as *"one-pot detection systems"*. Sometimes, more than one class of aptamers are used to stabilize NPs [4x]. Yang and co-workers [4k] described a *"one-pot detection system"* for ochratoxin A (OTA) where phosphate buffered saline (PBS), Mg^{2+}, OTA and the aptamer are mixed with AuNPs that can undergo salt-induced aggregation within 5 min [4k] (Fig. 15).

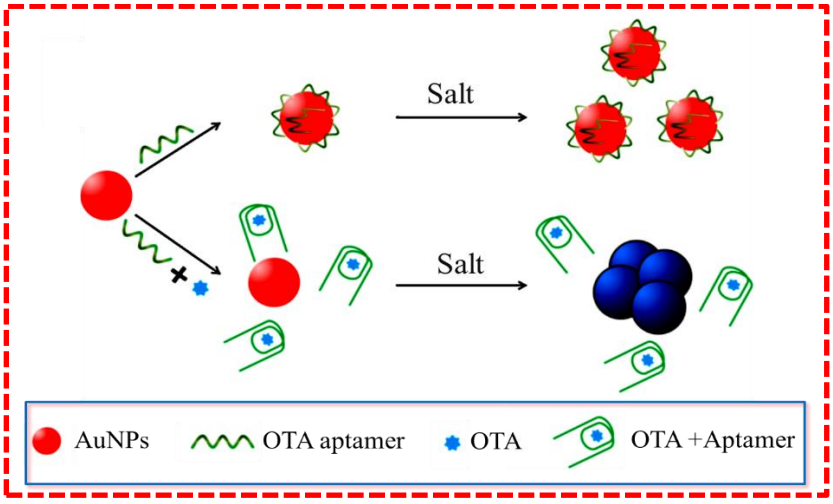

Fig. 15. *One-pot detection system of* ochratoxin A (OTA). The target is bound to the aptamer and upon salt addition, AuNP aggregation can be detected by the solution color change.

Although the method is different, the authors hypothesized that "the duly formed G-quadruplex structure could not protect AuNPs against salt-induced aggregation, and thus the color change from red to blue could be observed by the naked eye", as previously proposed by Wei *et al.* [5g] and Wang *et al.* [3e] for Type I and Type II detection systems. Interestingly the LOD is 20 nM, while the LDR from 20 to 625 nM [4k]. The major limitation of the Type III approach is that there is more than one source of electrostatic interactions that could change the solution color. For instance, if the metal is in excess, it will also contribute to the electrostatic interactions, and this

can only be prevented by having ssDNA in excess. Therefore selectivity is a major limiting factor for this approach.

5.4. TYPE IV: Multiplex Aptasensors

In this section, the systems that use more than one aptamer based on the previously described structure-switching strategies are described. In homogeneous multiplex aptasensors, more than one class of aptamer is used to stabilize NPs for detection of single or several targets [4x]. Several approaches are based on the likelihood that the target DNA molecules with one nucleotide mismatch have different melting temperatures, and therefore they can be distinguished by NPs disassociation based on temperature [6b, 6c, 6f, 7e, 17a, 50]. A typical example of such a DNA sensor was reported by Mirkin and co-workers, in which the target DNA molecules triggered AuNPs aggregation by hybridizing two complementary DNA strands on the AuNPs [18].

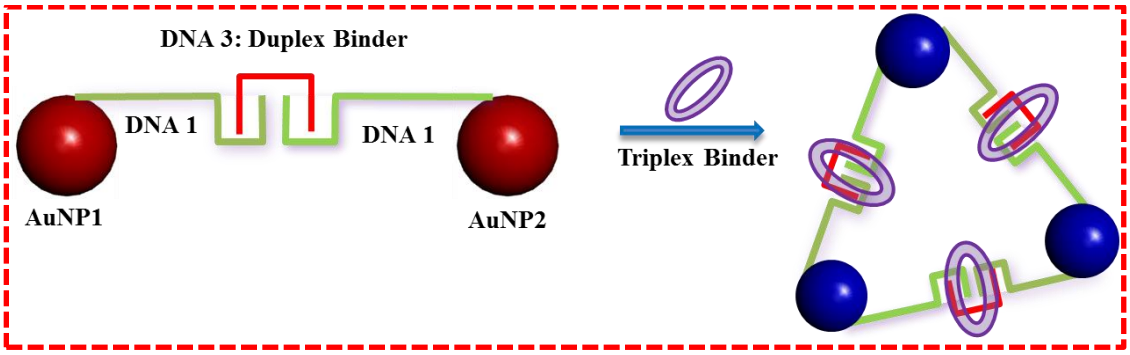

Fig. 16. Representation of the structure and color change of nano-assemblies in the presence of a triplex binding agent at room temperature [42].

Another assay includes AuNPs of different sizes (AuNP1 and AuNP2) that are functionalized with non-complementary DNAs (3' or 5' pyrimidine-rich thiol-modified oligonucleotides) (Fig. 16). Functionalized AuNP1 and AuNP2 are then cross-linked with another complementary DNA to form non-aggregating duplexes [42]. Introduction of a triplex binding agent induces triplex formation through base hydrogen bonds and consequently, reversible NP aggregation that result in a red-to-blue color change [42]. Analysis of the aggregate melting properties in terms of cooperative binding theories suggests a lower DNA surface coverage on AgNPs functionalized with 12 mer-thiolated homo-oligonucleotides containing only adenine (AgNPs/ST) than that on

AuNPs functionalized with 12mer-thiolated homo-oligonucleotides containing only thymine (AuNPs/ST), while exhibiting changes that are significantly different from those of AuNPs upon hybridization [51].

Interestingly, Sato *et, al.* [48] demonstrated that ssDNA-AuNPs have different stability against salt-induced aggregation in the presence of complementary DNA, although there is no triplex binder [48]. Using a similar assay format, Zhao *et al.* configured oligonucleotide-modified AuNPs duplexes with a short complementary oligonucleotide. Upon addition of adenosine (the target), the aptamer switches its structure from a DNA duplex to an aptamer/target complex, because the aptamer preferentially binds to the target molecule [7b]. Importantly, the aptamer on NP surfaces must retain its switching capability [7b, 18, 42, 48]. Erickson's group [15] developed a multiplexed one-pot detection system for Kaposi's sarcoma-associated herpesvirus (KSHV) and Bartonella using both AuNPs and AgNPs. Specifically, when the Bartonella-targeted DNA (BA-DNA) is introduced in the solution, AgNPs aggregate and the solution turns pink, more dependent on the SRP characteristics of non-aggregated AuNPs. When KSHV-DNA was introduced, AuNP aggregate and the solution changes to a murky yellow-orange color, more dependent on AgNP aggregation [15]. The multi-color change tuning of AuNPs and AgNPs gave LODs down to 1 nM and 2 nM, respectively [15].

Niu et *al*. [4x] used more than one class of aptamers to stabilize AuNPs (Type I). Specifically, a kanamycin-specific aptamer (750 nM), a sulfadimethoxine-specific aptamer (250 nM) and an adenosine-specific aptamer (500 nM) are mixed (1:1:1 volume ratio) and adsorbed directly onto the surface of unmodified AuNPs by electrostatic interaction. Upon addition of any of the three targets, the conformation of the corresponding aptamer changes from a random coil structure to a rigid folded structure that cannot adsorb and stabilize AuNPs [4x]. Although this looks more like a type III system, more than one aptamer is present and the reaction does not proceed sequentially.

Ultimately, multiplex systems are not straight forward because multiplex detection largely depends on the concentration of each aptamer and the buffer used for the aptamer reaction with its target [4x]. Moreover, all the aptamers in solution can be adsorbed onto the NP surface; however, the level of adsorption also depends on the neighboring aptamers. For this reason, the use of aptamers with short sequences gives better adsorption yields. It has been shown that changing the length of the ssDNA sequences yields different particle dispersion profiles on unmodified AuNPs, and that short DNA sequences might improve the colloidal

stability against salt-induced aggregation [4l, 4v, 6e]. Most importantly, the aptamer on the NP surface must retain its switching capability and for this reason the switching capability of the structures with aptamers is a key factor that determine the LOD of the assay [7b].

The multiplex type of aptamers has proven to be useful for enzyme activity and inhibitor assays.

5.5. Nanoparticle-based enzyme assays

NPs can be used also to improve colorimetric assays of enzymes [52]. In these systems, the substrate for the target enzyme should also be a suitable NP stabilizer. For instance, it should be stable at high salt concentration (approximately 100 mM). Moreover, a charged molecule that can provide electrostatic and steric stabilization is likely to yield better selectivity. The strong interaction between amino groups and AuNPs surfaces has been well confirmed and the bond energy is comparable to that of a thiol–Au bond. The rapid aggregation induced by the non-crosslinking process is a useful approach for enzyme inhibition-based colorimetric screening, as shown by several studies using assays that rely on polymeric aggregates of DNA-functionalized AuNPs (DNA-AuNPs) with DNA-duplex interconnections [7e, 7j, 7k]. Mirkin's group functionalized two separate batches of 13-nm AuNPs with two different thiol-modified oligonucleotide strands (DNA-1: 5'-CTCCCTAATAACAATTTATAACTATTCCTA-A10-SH-3', and DNA-2: 5'-TAGGAATAGTTATAAATTGTTATTAGGGAG-A10- SH-3') (blue and red ribbons, respectively, in Fig. 17) [7e].

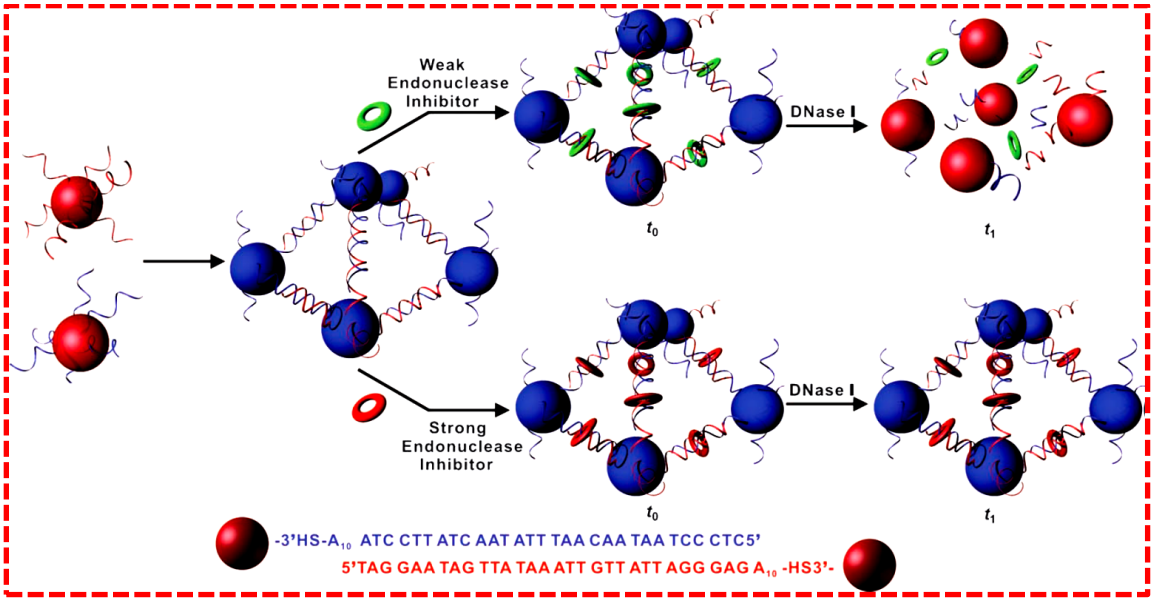

Fig. 17. Aggregation and dissociation of the DNA-AuNPs probe used in the colorimetric screening of endonuclease inhibitors. The probe consists of spherical AuNPs functionalized with two complimentary oligonucleotides (blue and red ribbons). Individual NPs (red) aggregate into a cross-

linked network of NPs (blue) through hybridization of their oligonucleotide chains. Upon addition of DNase I, the aggregates remain intact longer in the presence of a strong endonuclease inhibitor [7e].

The endonuclease (DNase I) degrades the DNA-duplex interconnections and NPs are released, thus generating a red color [7e] (Fig 17). In the presence of inhibitors, the DNase 1 activity is decreased and the aggregates are strongly hydrolyzed (T_H) . Consequently, the time required for the color change is much longer. Most importantly, strong inhibitors (in contrast to weak inhibitors) hinder DNase I activity to such an extent that the color change is no longer possible [7e]. In their method, endonucleases cleaves dsDNA in the absence of inhibitors and cross-linked AuNPs can separate into single AuNP molecules, as indicated by the instant color change, from blue to red. With this approach, the inhibitor performance can be directly evaluated. Similar observations were made using a system that includes a single type of DNA-AuNPs probe and an appropriate oligonucleotide linker that can hybridize with the DNA probe. The linker was designed to contain a self-complementary region that can form a duplex structure with a base-pair overlap that contains the recognition sites and overhanging 3'-ends [7k] (Fig. 18). Significant color change is observed when the endonuclease (DNA methyltransferase, DNA MTase) degrades the DNA duplex [7k].

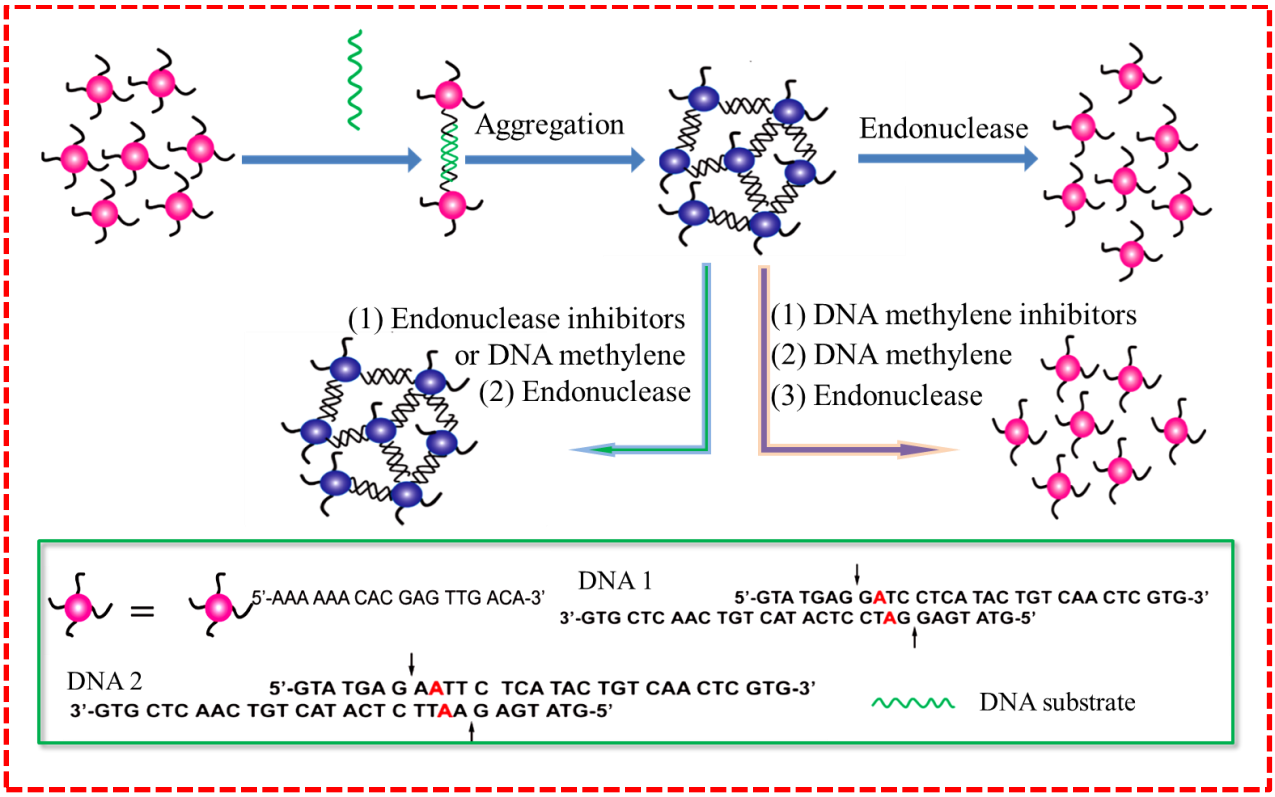

743

744 **Fig. 18. (A) Schematic representation of the assay to assess endonuclease and methyltransferase**
745 **activity and inhibition. (B) Sequences of the DNA probe, DNA-1 (recognition site for the**
746 **DpnII/Dam MTase) and DNA-2 (recognition site for the EcoRI/EcoRI MTase). The arrows show**
747 **the cleavage sites, and the red letters indicate the methylation sites [7k].**
748

749 Although highly selective and more sensitive than conventional methods, this visual inspection
750 assay is limited for the preparation of probes by functionalizing two separate AuNP batches with
751 two different thiol-modified oligonucleotide strands. On the other hand, this approach can be
752 used for most endonucleases by simply changing the recognition sequence in the linker DNA [7k].
753 For instance, similar assays were used for assessing adenosine triphosphate (ATP)
754 dephosphorylation by calf intestine alkaline phosphatase (CIAP) and peptide phosphorylation by
755 protein kinase A (PKA). ATP can protect AgNPs from salt-induced aggregation only in the
756 absence of enzymes. Phosphorylation and dephosphorylation can be readily detected by the color
757 change of AgNPs (CIAP LOD: 1 unit mL^{-1}, and PKA LOD: 0.022 unit mL^{-1}) [7h]. Zhao and co-
758 workers took advantage of the non-crosslinking AuNPs aggregation phenomenon to develop a
759 simple colorimetric assay for monitoring an enzymatic dephosphorylation reaction, where ATP
760 is converted into adenosine by CIAP [7a]. AuNPs capped by adenosine 5'-monophosphate
761 (AMP), adenosine 5'-diphosphate (ADP), or adenosine 5'-triphosphate (ATP) are progressively

762 more stable than bare AuNPs, but their stability gradually decreases (and thus the color of the
763 solution) with the dephosphorylation process [7a]. Likewise, Choi *et al.* [40] described an alkaline
764 phosphatase assay based on AuNPs aggregation [40]. To develop an adenosine deaminase assay,
765 Zhang and co-workers hypothesized that the interaction between adenosine amino group and
766 AuNPs surface will displace the weakly bound citrate ions from the AuNPs surface and diminish
767 the stability of citrate-capped AuNPs, resulting in the aggregation of AuNPs in the presence of
768 NaCl and a corresponding red to blue color change. Adenosine, guanosine and cytidine
769 (molecules that contain amino groups) strongly interact with AuNPs, causing aggregation.
770 Conversely, inosine, thymidine and uridine have negligible effects on AuNPs stability, therefore
771 the solution remains red because of the stronger electrostatic repulsion between negatively-
772 charged AuNPs [8]. Xinhui *et al.* described a suitable method for nucleases, such as the S1
773 nuclease [7j]. In the presence of nucleases and their substrates, unmodified AuNPs are stabilized
774 by dNMPs at high salt concentration and the solution remains red. Conversely, in the absence of
775 nucleases or substrates, the unmodified AuNP solution turns blue at high salt concentration due
776 to aggregate formation [7j].

777 Xu and co-workers developed a colorimetric assay to screen for inhibitors of several
778 kinases with the same type of NPs [7d] (Fig. 19). The method takes advantage of peptide-capped
779 NPs, in which 10% of peptide ligands carry an extension that is the substrate for a specific kinase
780 (PKA or calmodulin-dependent kinase II, CaM KII). Using ɣ-biotin-ATP as a co-substrate, the
781 kinase reaction results in substrate-AuNP biotinylation.

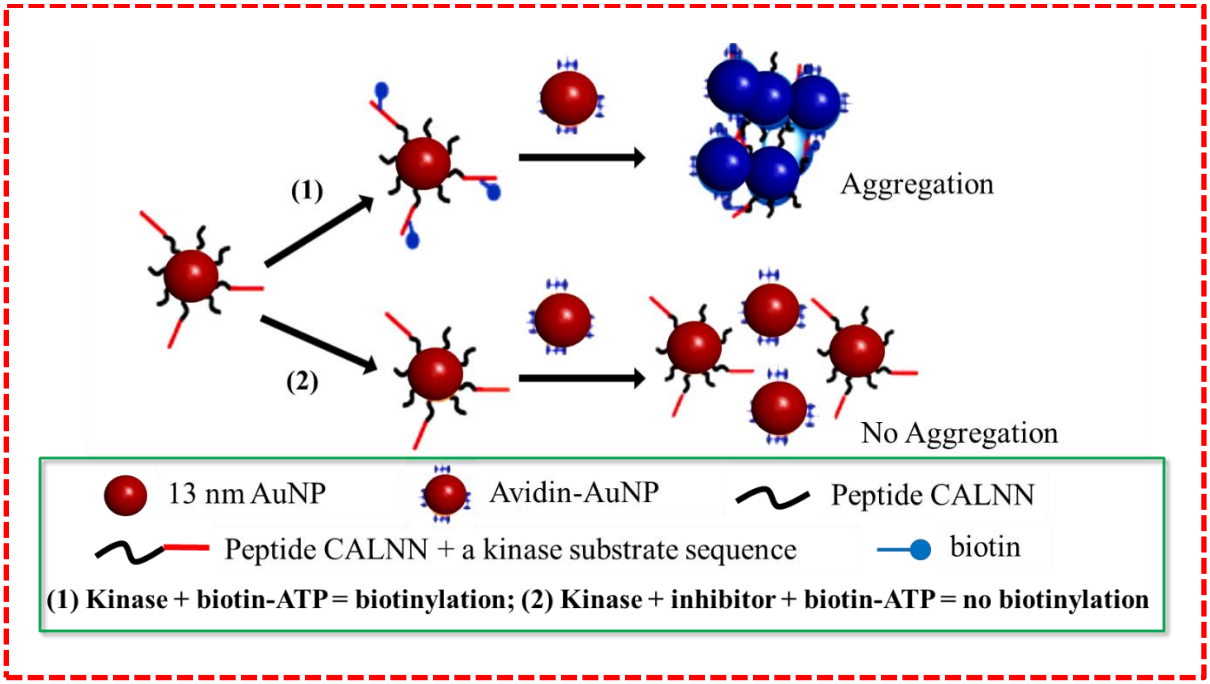

Fig. 19. Schematic representation of phosphorylation/biotinylation of substrate-NPs followed by addition of avidin-modified NPs, in the presence and absence of a kinase inhibitor [7d]

When biotinylated substrate-AuNPs are mixed with avidin-AuNPs, they immediately aggregate due to the specific binding between avidin and biotin [7d]. Similarly, Wei *et al.* [7h] reported that in the absence of the kinase, or in the presence of an efficient inhibitor, no observable color change occurs after addition of avidin-modified NPs, and the solutions are indefinitely stable without showing signs of aggregation [7d]. Furthermore, a hydrolysis-based colorimetric assay for acetylcholinesterase (AChE) was developed based on the finding that AChE can catalyze acetylthiocholine hydrolysis into thiocholine [45]. AChE and acetylthiocoline are added in the AuNP solution, the generated thiocholine can take the place of citrate on the AuNP surface, promoting NP aggregation and a change of color from red to gray. Addition also of the AChE inhibitor tacrine (1,2,3,4-tetrahydroacridin-9-amine) leads to less AuNP aggregation and a slower color change [45]. Uehara *et al.* [43] reported that gold nanocomposites conjugated with a thermo-responsive copolymer can be used in a colorimetric assay to quantify the activity of aminopeptidase N (APN). By heating the solution, the assembled gold nanocomposites disassemble and the solution color change from blue, purple to red. This process is inhibited by cysteine, therefore the enzymatic decomposition of cysteinylglycine into cysteine and glycine by APN can be monitored [43].

Tiwari *et al.* hypothesized that particles could be used for the detection of the hydrolytic activity of penicillin G acylase (PGA) on penicillin G. This hydrolysis reaction leads to a shift in the surface plasmon band of AuNPs from 527 to 545 nm accompanied by a solution color change from red to blue. The presence of 0.007 mg ml^{-1} PGA can be detected [7m]. The enzyme is known to hinder the salt-induced NP aggregation. Xie and co-workers found that DNA-RNA duplexes cannot stabilize unmodified NPs at a certain salt concentration, a typical type II approach. However, addition of the active HIV-1 RNase H enzyme leads to the specific cleavage of RNA strands into RNA fragments and ssDNAs that can stabilize NPs against salt-induced aggregation [7o]. In an assay for glycosidases based on self-immolative elimination to release amines, functionalized trigger-AuNPs aggregate by electrostatic attraction upon cleavage of the trigger. The assay gives LODs for β-galactosidase (Gal) and β-glucosidase (Glc) of 9.2 and 22.3 nM, respectively, at 20 min, and they improve slightly over time [44]. The functionalized AuNPs (2.0 nM), which were capped with the enzyme substrate ligand Gal-Lip (or Glc-Lip) and lipoic acid at a ratio of 1:1, showed a typical SPR peak at 521 nm (i.e., a red shift of 2 nm compared with citrate-AuNPs) and good stability in PBS. The respective addition of Gal or Glc caused a time-dependent decrease of the peak absorbance induced by NP aggregation that could be observed by naked eye.

Two different systems (the DNA endonuclease DNase I and the Pb^{2+}-dependent RNA-cleaving DNA enzyme 8-17) were chosen to demonstrate the utility of an assay for the detection of metal ions and enzyme activities based on rapid NP aggregation driven by van der Waals attraction [7i] (Fig. 20).

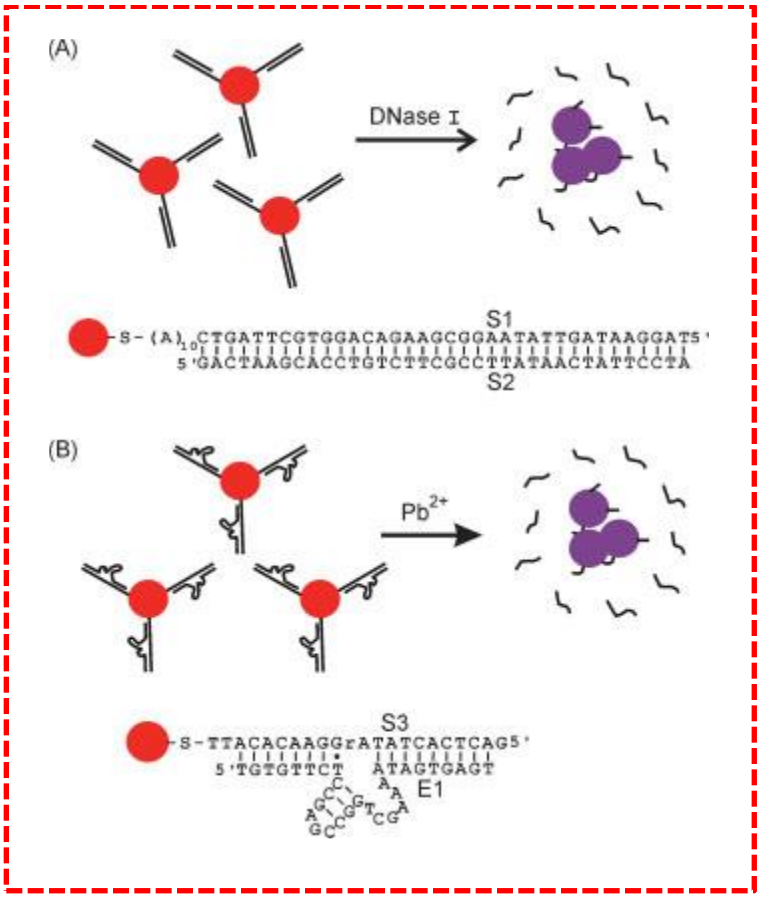

Fig. 20. Schematic illustration of AuNP aggregation and color change triggered by the enzymatic cleavage of DNA on AuNPs. Before enzymatic cleavage, DNA-modified AuNPs are stable at a relatively high salt concentration, due to their electrostatic and steric stabilization. DNA removal from the AuNP surface by enzymatic cleavage destabilizes AuNPs and results in their rapid aggregation. A) Cleavage of a DNA duplex by DNase I. B) Pb^{2+}-mediated cleavage of an RNA-containing DNA substrate by the 8-17 DNA enzyme [7i].

The authors reasoned that the removal from the NP surface of DNA strands, which serve as electrostatic and steric stabilizers at relatively high salt concentrations (e.g., 40 mM $MgCl_2$), should result in AuNPs destabilization and aggregation, a process driven by van der Waals attraction [7i]. Indeed, addition of 100 mM Pb^{2+} generated a rapid red-to-purple color change at room temperature [7i].

AuNPs generation induced by neurotransmitters can be used to analyze the activity of tyrosinase, an enzyme that catalyzes the O_2-induced hydroxylation of tyrosine to L-DOPA [4b]. As tyrosinase concentration increases, the SPR bands of NPs are intensified and slightly blue-shifted, suggesting that larger particles are formed, and small Au nanoclusters enlarged [4b]. This system can be used for the sensitive detection of dopamine, L-DOPA and noradrenaline (LOD of

2.5 µM) and adrenaline (0.2 µM) that act as active reducing agents for Au-NP generation of Au-NPs [4b].

Colorimetric aptasensors for the quantitative analysis of abrin using catalytic AuNPs were reported for the first time by Zhang *et al*. and Wu *et al*. The AuNP peroxidase-like activity can catalyze 3, 3, 5, 5-tetramethylbenzidine (TMB) formation in the presence of H_2O_2, leading to a color change [4a, 7p]. Particularly, Song *et al.* [7k] quote the work by Mirkin's group [7e] and say that the rest of the methods eliminate the binder use of different DNAs to obtain functionalized-NP1 and functionalized-NP2. However, such method requires cumbersome preparation of modified NPs and the formation of crosslinked NPs. Thus, it is not suitable for high-throughput screening.

Crosslinking also offers a unique selectivity in reversibility of NP aggregation, where analytes dissociate the cross-linker and re-disperse the NP aggregates to their original color. For instance, Lu and co-workers described detection assays for Pb^{2+}, adenosine and cocaine where DNA molecules with a single RNA linkage serve as cross-linkers that bring complementary DNA-AuNPs into aggregates. The DNA enzyme catalyzes the specific hydrolytic cleavage of the substrate strand that disrupts the NP assembly, changing the color from purple to red and thus indicating the presence of Pb^{2+} [3a, 7c].

Zhao and co-workers speculated that if the substrate and product of an enzymatic reaction affect differently AuNP stability by changing their electrophoretic properties, such a reaction can be monitored colorimetrically and the enzymatic activity can therefore be determined [7a].

6. Core-Shell Nanoparticles and Ratios

Core–shell nanoparticles (CSNs) are a class of nanostructured materials that have recently received increased attention owing to their interesting properties and broad range of applications in catalysis, biology, materials chemistry and sensors. By rationally tuning the cores as well as the shells of such materials (ratios), a range of core–shell nanoparticles can be produced. In this review, the combination of gold and silver enhancement, an electron-dense deposits that can be read by a simple colorimetric array workstation [6d]. However, Cao *et al*. stated that AgNPs cannot be effectively passivated by alkylthiol-modified-oligonucleotides using the protocols for modifying AuNPs, because they irreversibly aggregate when heated in a solution with 0.05MNaCl, the concentration needed for DNA hybridization [17b]. For this reason,

an Au shell can be grown on AgNP, forming a particle with an Au outer surface (3.1 ± 0.6 Å). This surface can be easily modified with alkylthiol-oligonucleotides and indefinitely suspended in high salt solutions. Ag/Au core-shell NPs retain the optical properties of the silver core, but have optical properties different from pure gold NPs, thus providing another "color" option for 30-mer DNA target-directed colorimetric detection [6f, 17b].

By taking advantage of their reversible aggregation and melting nature, oligonucleotide-modified Ag@SiO_2 nano-probes can be prepared by using 5' TCT-CAA-CTC-GTA-$(CH_2)7$-NH_2 3' and non-complementary oligonucleotides with a 5' TAC-GAG-TTG-AGA-GAG-TGC-CCA-CAT3' sequence in which no hybridization product was reported [50]. The high stability of oligo-modified Ag@SiO_2 nano-probes at elevated temperatures (30-70°C) was confirmed by the absence of peak shift and of broadening of well-dispersed nano-probes in their UV-Vis spectra after long heating. The fast hybridization kinetics of the resulting Ag@SiO_2 nano-probes with complementary target oligonucleotides render them very useful for fast colorimetric detection based on the sequence-specific hybridization properties of DNA [50].

CSNs can also be used to introduce a second colorimetric change, distinct from the gold system, for monitoring two different oligonucleotide targets in one sample [17b]. For instance, when lactose-stabilized AuNPs are mixed with mannose (2-mercaptoethyl R-D-mannopyranoside)-stabilized AgNPs [2], addition of concanavalin A (Con A) leads to the aggregation only of mannose-stabilized AgNPs, thereby demonstrating the system selectivity. Limited non-specific interaction occurs with lectin Con A, thereby enabling the subsequent specific interaction with the lectin from *Ricinus Communis* Agglutinin (RCA120). Although mannose-stabilized AgNPs show a longer LDR and faster reaction kinetics for the target lectin, mannose-stabilized AuNPs provide the most sensitive bioassay [2].

Nevertheless, the synthesis of the CSNs can be a daunting task for quick assays [4f].

7. Summary and outlook

The detection of metals and molecules based on bare-eye observable colorimetric changes depends on various parameters that are even more complex for macromolecules. The functional groups on the NP surface are very influential in various areas of research, such as sensor arrays and biosensor detection. Overall in any given condition, both thiols and nucleotides compete for adsorption sites, and the equilibrium shifts towards thiols adsorption as the salt concentration

increases. Therefore, nucleotide adsorption could be completely eliminated after being 'crowded out' (steric hindrance) as more thiols are adsorbed onto the metal. In one-pot detection approach (where nanoparticles, analyte, DNA or enzyme are mixed together) qualitative analyses is deemed imprecise because the color changes are not only due to the analyte, as they could be triggered also by DNA or enzyme adsorption to the NP surface.

Also, the multiplex aptasensors have some limitations. For instance, it is not possible to determine which target is detected when the sample gives a positive result (change of color). While enzyme-assisted assays have a huge potential for many applications in biomedicine and bio-imaging, the application of the described *in vivo* techniques faces formidable challenges. Indeed, the interactions of NPs with enzyme molecules are not yet fully understood.

Through the review, there are viable approaches that have been introduced, Firstly, aptamer truncation to overcome the limitations due to the DNA length, while maintaining the original binding affinity. Secondly, overcoming the limitation imposed by the stability of AgNPs by coating them with a thin layer of gold to produce a core–shell structure that retains the spectrophotometric signature of the silver core. Thirdly, use of chemometric approaches provides synergy in colorimetric discrimination or classification of small molecules and macromolecules.

Overall, the AuNP-based colorimetric aptasensors are currently used for many analytes, largely because of the ease of detection, high sensitivity and potential for high-throughput analysis. Moreover, the synergy between chemometrics and biotechnology selectivity narrows the gap for the development of smart apta-based colorimetric sensing devices. In any case, careful interpretation of the findings is critical because the colorimetric changes are not general or universal, suggesting that they are highly dependent on the analytes and matrices.

REFERENCES

[1] a) V. Chegel, O. Rachkov, A. Lopatynskyi, S. Ishihara, I. Yanchuk, Y. Nemoto, J. P. Hill, K. Ariga, *J. Phys. Chem. C* **2012**, 116, 2683; b) T. C. Prathna, N. Chandrasekaran, A. Mukherjee, *Colloids Surf. A Physicochem. Eng. Asp.* **2011**, 390, 216; c) V. Amendola, O. Bakr, F. Stellacci, *Plasmonics* **2010**, 5, 85; d) W. Wang, M. Yang, Z. Wang, J. Yan, C. Liu, *RSC Adv.* **2014**, 4, 63079.

[2] C. L. Schofield, A. H. Haines, R. A. Field, D. A. Russell, *Langmuir* **2006**, 22, 6707.

[3] a) J. Liu, Y. Lu, *Journal of the American Chemical Society* **2003**, 125, 6642; b) A. Ravindran, V. Mani, N. Chandrasekaran, A. Mukherjee, *Talanta* **2011**, 85, 533; c) S. Hajizadeh, K. Farhadi, M. Forough, R. Molaei, *Anal. Methods* **2012**, 4, 1747; d) J. M. Slocik, J. S. Zabinski, D. M. Phillips, R. R. Naik, *Small* **2008**, 4, 548; e) L. Wang, X. Liu, X. Hu, S. Song, C. Fan, *Chem. Comm.* **2006**, 3780; f) F. Xia, X. Zuo, R. Yang, Y. Xiao, D. Kang, A. Vallée-Bélisle, X.

Gong, J. D. Yuen, B. B. Y. Hsu, A. J. Heeger, K. W. Plaxco, *Proc. Natl. Acad. Sci.* **2010**, 107, 10837; g) F. Wang, Y. Wu, S. Zhan, L. He, W. Zhi, X. Zhou, P. Zhou, *Aust. J. Chem.* **2013**, 66, 113.

[4] a) Z.-S. Wu, S.-B. Zhang, M.-M. Guo, C.-R. Chen, G.-L. Shen, R.-Q. Yu, *Anal. Chim. Acta* **2007**, 584, 122; b) R. Baron, M. Zayats, I. Willner, *Anal. Chem.* **2005**, 77, 1566; c) J. Liu, Y. Lu, *Angew. Chem. Int. Ed.* **2006**, 45, 90; d) J.-S. Lee, P. A. Ulmann, M. S. Han, C. A. Mirkin, *Nano Lett.* **2008**, 8, 529; e) Z. Chen, S. Luo, C. Liu, Q. Cai, *Anal. Bioanal. Chem.* **2009**, 395, 489; f) X. Xu, J. Wang, F. Yang, K. Jiao, X. Yang, *Small* **2009**, 5, 2669; g) Y. S. Kim, J. H. Kim, I. A. Kim, S. J. Lee, J. Jurng, M. B. Gu, *Biosens. Bioelectron.* **2010**, 26, 1644; h) Y. Zhang, B. Li, X. Chen, *Microchim. Acta* **2010**, 168, 107; i) Y. Zhang, B. Li, C. Xu, *Analyst* **2010**, 135, 1579; j) K.-M. Song, M. Cho, H. Jo, K. Min, S. H. Jeon, T. Kim, M. S. Han, J. K. Ku, C. Ban, *Anal. BioChem.* **2011**, 415, 175; k) C. Yang, Y. Wang, J.-L. Marty, X. Yang, *Biosens. Bioelectron.* **2011**, 26, 2724; l) K.-M. Song, E. Jeong, W. Jeon, M. Cho, C. Ban, *Anal. Bioanal. Chem.* **2012**, 402, 2153; m) J. Athilakshmi, M. Mohan, D. K. Chand, *Tetrahedron Lett.* **2013**, 54, 427; n) A. Chen, X. Jiang, W. Zhang, G. Chen, Y. Zhao, T. M. Tunio, J. Liu, Z. Lv, C. Li, S. Yang, *Biosens. Bioelectron.* **2013**, 42, 419; o) H. Gao, W. Shen, C. Lu, H. Liang, Q. Yuan, *Talanta* **2013**, 115, 1; p) A. Liu, Y. Zhang, W. Chen, X. Wang, F. Chen, *Eur. Food Res. Technol.* **2013**, 237, 323; q) Z. Mei, H. Chu, W. Chen, F. Xue, J. Liu, H. Xu, R. Zhang, L. Zheng, *Biosens. Bioelectron.* **2013**, 39, 26; r) S. Chen, H. Gao, W. Shen, C. Lu, Q. Yuan, *Sens. Actuator B-Chem.* **2014**, 190, 673; s) H.-H. Deng, C.-L. Wu, A.-L. Liu, G.-W. Li, W. Chen, X.-H. Lin, *Sens. Actuator B-Chem.* **2014**, 191, 479; t) C. Han, K. Xu, Q. Liu, X. Liu, J. Li, *Sens. Actuator B-Chem.* **2014**, 202, 574; u) S. Jongjinakool, K. Palasak, N. Bousod, S. Teepoo, *Energy Procedia* **2014**, 56, 10; v) Y. S. Kwon, N. H. Ahmad Raston, M. B. Gu, *Chem. Comm.* **2014**, 50, 40; w) W. Li, C. Pan, T. Hou, X. Wang, F. Li, *Anal. Methods* **2014**, 6, 1645; x) J. Liu, W. Bai, S. Niu, C. Zhu, S. Yang, A. Chen, *Sci. Rep.* **2014**, 4; y) L. Zhang, C. Xu, C. Liu, B. Li, *Anal. Chim. Acta* **2014**, 809, 123; z) I. E. Paul, A. Rajeshwari, T. C. Prathna, A. M. Raichur, N. Chandrasekaran, A. Mukherjee, *Anal. Methods* **2015**, 7, 1453; aa) A. Sarreshtehdar Emrani, N. M. Danesh, P. Lavaee, S. H. Jalalian, M. Ramezani, K. Abnous, S. M. Taghdisi, *Anal. Methods* **2015**; ab) K. V. Ragavan, L. S. Selvakumar, M. S. Thakur, *Chem. Comm.* **2013**, 49, 5960; ac) Y. Zhang, J. Jiang, M. Li, P. Gao, Y. Zhou, G. Zhang, S. Shuang, C. Dong, *Talanta* **2016**, 161, 520; ad) S. Wu, D. Li, J. Wang, Y. Zhao, S. Dong, X. Wang, *Sens. Actuator B-Chem.* **2017**, 238, 427.

[5] a) V. Pavlov, Y. Xiao, B. Shlyahovsky, I. Willner, *Journal of the American Chemical Society* **2004**, 126, 11768; b) C.-S. Tsai, T.-B. Yu, C.-T. Chen, *Chem. Comm.* **2005**, 4273; c) C.-C. Huang, Y.-F. Huang, Z. Cao, W. Tan, H.-T. Chang, *Anal. Chem.* **2005**, 77, 5735; d) J. Li, X. Chu, Y. Liu, J.-H. Jiang, Z. He, Z. Zhang, G. Shen, R.-Q. Yu, *Nucleic Acids Res.* **2005**, 33, e168; e) J.-M. Nam, K.-J. Jang, J. T. Groves, *Nat. Protocols* **2007**, 2, 1438; f) R.-Q. Liang, C.-Y. Tan, K.-C. Ruan, *J. Immunol. Methods* **2004**, 285, 157; g) H. Wei, B. Li, J. Li, E. Wang, S. Dong, *Chem. Comm.* **2007**, 3735; h) S. Siddhartha, D. Debabrata, *Nano-Micro Lett.* **2010**, 2, 164; i) M. Lepoitevin, M. Lemouel, M. Bechelany, J.-M. Janot, S. Balme, *Microchim. Acta* **2015**, 182, 1223; j) J. Mao, Y. Lu, N. Chang, J. Yang, S. Zhang, Y. Liu, *Biosens. Bioelectron.* **2016**, 86, 56.

[6] a) R. Kanjanawarut, X. Su, *Anal. Chem.* **2009**, 81, 6122; b) R. Elghanian, J. J. Storhoff, R. C. Mucic, R. L. Letsinger, C. A. Mirkin, *Science* **1997**, 277, 1078; c) J. J. Storhoff, R. Elghanian, R. C. Mucic, C. A. Mirkin, R. L. Letsinger, *Journal of the American Chemical Society* **1998**, 120, 1959; d) I. Alexandre, S. Hamels, S. Dufour, J. Collet, N. Zammatteo, F. De Longueville, J. L. Gala, J. Remacle, *Anal. BioChem.* **2001**, 295, 1; e) H. Li, L. Rothberg, *Proceedings of the National Academy of Sciences of the United States of America* **2004**, 101,

14036; f) Y. C. Cao, R. Jin, C. S. Thaxton, C. A. Mirkin, *Talanta* **2005**, 67, 449; g) Q. Shen, Z. Nie, M. Guo, C.-J. Zhong, B. Lin, W. Li, S. Yao, *Chem. Comm.* **2009**, 929.
[7] a) W. Zhao, W. Chiuman, J. C. F. Lam, M. A. Brook, Y. Li, *Chem. Comm.* **2007**, 3729; b) B. Liu, L. Wen, X. Zhao, *Mater. Chem. Phys.* **2007**, 106, 350; c) J. Liu, Y. Lu, *J. Fluoresc.* **2004**, 14, 343; d) Z. Wang, R. Lévy, D. G. Fernig, M. Brust, *Journal of the American Chemical Society* **2006**, 128, 2214; e) X. Xu, M. S. Han, C. A. Mirkin, *Angew. Chem* **2007**, 119, 3538; f) Y.-M. Chen, C.-J. Yu, T.-L. Cheng, W.-L. Tseng, *Langmuir* **2008**, 24, 3654; g) J. Oishi, Y. Asami, T. Mori, J.-H. Kang, T. Niidome, Y. Katayama, *Biomacromolecules* **2008**, 9, 2301; h) H. Wei, C. Chen, B. Han, E. Wang, *Anal. Chem.* **2008**, 80, 7051; i) W. Zhao, J. C. F. Lam, W. Chiuman, M. A. Brook, Y. Li, *Small* **2008**, 4, 810; j) X. Lou, Y. Xiao, Y. Wang, H. Mao, J. Zhao, *ChemBioChem* **2009**, 10, 1973; k) G. Song, C. Chen, J. Ren, X. Qu, *ACS Nano* **2009**, 3, 1183; l) C.-K. Chen, C.-C. Huang, H.-T. Chang, *Biosens. Bioelectron.* **2010**, 25, 1922; m) N. Tiwari, Rathore, A. , Prabhune, A. and Kulkarni, S., *Adv. Biosci. Biotechnol.* **2010**, 1, , 322; n) R. Cao, B. Li, Y. Zhang, Z. Zhang, *Chem. Comm.* **2011**, 47, 12301; o) X. Xie, W. Xu, T. Li, X. Liu, *Small* **2011**, 7, 1393; p) W. Zhang, Y. Tang, J. Liu, L. Jiang, W. Huang, F.-W. Huo, D. Tian, *J. Agric. Food Chem.* **2015**, 63, 39.
[8] L. Zhang, J. Zhao, J. Jiang, R. Yu, *Chem. Comm.* **2012**, 48, 10996.
[9] N. L. Rosi, C. A. Mirkin, *Chemical Reviews* **2005**, 105, 1547.
[10] C. Lee, M. A. Gaston, A. A. Weiss, P. Zhang, *Biosens. Bioelectron.* **2013**, 42, 236.
[11] a) Y. Yu, Y. Hong, Y. Wang, X. Sun, B. Liu, *Sens. Actuator B-Chem.* **2017**, 239, 865; b) F. Ghasemi, M. R. Hormozi-Nezhad, M. Mahmoudi, *Anal. Chim. Acta* **2015**, 882, 58; c) L. Li, B. Li, *Analyst* **2009**, 134, 1361; d) N. Fahimi-Kashani, M. R. Hormozi-Nezhad, *Anal. Chem.* **2016**, 88, 8099.
[12] Z. Chen, C. Zhang, T. Zhou, H. Ma, *Microchim. Acta* **2015**, 182, 1003.
[13] S. Basu, S. Jana, S. Pande, T. Pal, *J. Colloid Interface Sci.* **2008**, 321, 288.
[14] B. C. Vidal Jr, T. C. Deivaraj, J. Yang, H.-P. Too, G.-M. Chow, L. M. Gan, J. Y. Lee, *New J. Chem.* **2005**, 29, 812.
[15] M. Mancuso, L. Jiang, E. Cesarman, D. Erickson, *Nanoscale* **2013**, 5, 1678.
[16] X. Zhang, M. R. Servos, J. Liu, *Chem. Comm.* **2012**, 48, 10114.
[17] a) J.-S. Lee, A. K. R. Lytton-Jean, S. J. Hurst, C. A. Mirkin, *Nano Lett.* **2007**, 7, 2112; b) Cao, R. Jin, C. A. Mirkin, *Journal of the American Chemical Society* **2001**, 123, 7961.
[18] C. A. Mirkin, R. L. Letsinger, R. C. Mucic, J. J. Storhoff, *Nature* **1996**, 382, 607.
[19] G. Mie, *Ann. Phys.* **1908**, 330, 377.
[20] S. Kundu, *Phys. Chem. Chem. Phys.* **2013**, 15, 14107.
[21] a) V. Banerjee, K. P. Das, *Colloids Surf. B* **2013**, 111, 71; b) X. Zhao, R. Liu, Y. Teng, X. Liu, *Sci Total Environ* **2011**, 409, 892; c) C. Bhan, R. Mandlewala, A. Gebregeorgis, D. Raghavan, *Langmuir* **2012**, 28, 17043; d) C. Bhan, T. L. Brower, D. Raghavan, *J. Colloid Interface Sci.* **2013**, 402, 40.
[22] W. Zhao, M. A. Brook, Y. Li, *ChemBioChem* **2008**, 9, 2363.
[23] Q. Qian, J. Deng, D. Wang, L. Yang, P. Yu, L. Mao, *Anal. Chem.* **2012**, 84, 9579.
[24] H. Chen, W. Hu, C. M. Li, *Sens. Actuator B-Chem.* **2015**, 215, 421.
[25] S. Watanabe, K. Yoshida, K. Shinkawa, D. Kumagawa, H. Seguchi, *Colloids Surf. B* **2010**, 81, 570.
[26] Y.-J. Chuang, X. Zhou, Z. Pan, C. Turchi, *Biochem. Biophys. Res. Commun.* **2009**, 389, 22.
[27] Y. Zheng, Y. Wang, X. Yang, *Sens. Actuator B-Chem.* **2011**, 156, 95.

[28] J.-J. Feng, H. Guo, Y.-F. Li, Y.-H. Wang, W.-Y. Chen, A.-J. Wang, *ACS Appl. Mater. Interfaces* **2013**, 5, 1226.
[29] H. Su, B. Sun, L. Chen, Z. Xu, S. Ai, *Anal. Methods* **2012**, 4, 3981.
[30] K. Rawat, S. Kailasa, *Microchim. Acta* **2014**, 181, 1917.
[31] W. Zhao, W. Chiuman, M. A. Brook, Y. Li, *ChemBioChem* **2007**, 8, 727.
[32] a) S. Aryal, R. B.K.C, N. Dharmaraj, N. Bhattarai, C. H. Kim, H. Y. Kim, *Spectrochimica Acta Part A: Molecular and Biomolecular Spectroscopy* **2006**, 63, 160; b) A. Kuhnle, T. R. Linderoth, B. Hammer, F. Besenbacher, *Nature* **2002**, 415, 891.
[33] G. Song, C. Xu, B. Li, *Sens. Actuator B-Chem.* **2015**, 215, 504.
[34] Y. Sun, H. Zhao, I. Boussouar, F. Zhang, D. Tian, H. Li, *Sens. Actuator B-Chem.* **2015**, 216, 235.
[35] W. Xue, G. Zhang, D. Zhang, *Analyst* **2011**, 136, 3136.
[36] C. Guarise, L. Pasquato, V. De Filippis, P. Scrimin, *Proceedings of the National Academy of Sciences of the United States of America* **2006**, 103, 3978.
[37] S. Abdul Rahman, R. Saadun, N. E. Azmi, N. Ariffin, J. Abdullah, N. A. Yusof, H. Sidek, R. Hajian, *J. Nanomater.* **2014**, 2014, 5.
[38] F. Ghasemi, M. R. Hormozi-Nezhad, M. Mahmoudi, *Analytica Chimica Acta* **2015**, doi:10.1016/j.aca.2015.04.011.
[39] J. Mehta, B. Van Dorst, E. Rouah-Martin, W. Herrebout, M.-L. Scippo, R. Blust, J. Robbens, *Journal of Biotechnology* **2011**, 155, 361.
[40] Y. Choi, N.-H. Ho, C.-H. Tung, *Angew. Chem. Int. Ed.* **2007**, 46, 707.
[41] R. Liu, R. Liew, J. Zhou, B. Xing, *Angew. Chem. Int. Ed.* **2007**, 46, 8799.
[42] M. S. Han, A. K. R. Lytton-Jean, C. A. Mirkin, *Journal of the American Chemical Society* **2006**, 128, 4954.
[43] N. Uehara, M. Fujita, T. Shimizu, *Anal. Sci.* **2009**, 25, 267.
[44] Z. Zeng, S. Mizukami, K. Kikuchi, *Anal. Chem.* **2012**, 84, 9089.
[45] M. Wang, X. Gu, G. Zhang, D. Zhang, D. Zhu, *Langmuir* **2009**, 25, 2504.
[46] J. Hu, P. Ni, H. Dai, Y. Sun, Y. Wang, s. jiang, Z. Li, *Analyst* **2015**, 140, 3581.
[47] T. A. Taton, C. A. Mirkin, R. L. Letsinger, *Science* **2000**, 289, 1757.
[48] K. Sato, K. Hosokawa, M. Maeda, *Journal of the American Chemical Society* **2003**, 125, 8102.
[49] M. Famulok, G. Mayer, *Nature* **2006**, 439, 666.
[50] S. Liu, Z. Zhang, M. Han, *Anal. Chem.* **2005**, 77, 2595.
[51] I. Tokareva, E. Hutter, *Journal of the American Chemical Society* **2004**, 126, 15784.
[52] X. Xie, W. Xu, X. Liu, *Acc. Chem. Res.* **2012**, 45, 1511.